

**MASARYKOVA
UNIVERZITA**

Přírodovědecká fakulta
Ústav teoretické fyziky a astrofyziky

**Systematický výzkum horkých atmosfér
obklopujících S0 galaxie**

Diplomová práce

Anna Juráňová

Vedoucí práce: doc. Mgr. Norbert Werner, Ph.D.

Brno 2019

Bibliografický záznam

Autorka: Bc. Anna Juráňová
Přírodovědecká fakulta, Masarykova univerzita
Ústav teoretické fyziky a astrofyziky

Název práce: Systematický výzkum horkých atmosfér
obklopujících S0 galaxie

Studijní program: Fyzika

Studijní obor: Teoretická fyzika a astrofyzika

Vedoucí práce: doc. Mgr. Norbert Werner, Ph.D.

Akademický rok: 2018/2019

Počet stran: ix + 59

Klíčová slova: čočkovité galaxie, aktivní galaxie,
rentgenová spektroskopie, horký plyn

Bibliographic Entry

Author: Bc. Anna Juráňová
Faculty of Science, Masaryk University
Department of Theoretical Physics and
Astrophysics

Title of Thesis: A systematic study of the hot gaseous
atmospheres of S0 galaxies

Degree Programme: Physics

Field of study: Theoretical Physics and Astrophysics

Supervisor: doc. Mgr. Norbert Werner, Ph.D.

Academic Year: 2018/2019

Number of Pages: ix + 59

Keywords: lenticular galaxies, active galaxies,
X-ray spectroscopy, hot gas

Abstrakt

Řada masivních eliptických a čočkovitých galaxií, včetně těch s nezanedbatelným momentem hybnosti, je prostoupena plynem o teplotách v řádu milionů kelvinů. Studie procesů formujících termodynamický stav horkého plynu v nerotujících galaxiích jsou publikovány již několik desítek let, avšak fyzikální vlastnosti horkých atmosfér těch rotujících dosud nebyly systematicky analyzovány. V této práci, zaměřené právě na studium vlastností horkého plynu v rychle rotujících čočkovitých galaxiích, se zabýváme analýzou pozorování rentgenové observatoře *XMM-Newton*. Z měření vyplývá, že entropie je v centrálních oblastech atmosfér rotujících galaxií zvýšená a její radiální nárůst je pozvolný, což ve srovnání s nerotujícími objekty odpovídá jejich efektivnějšímu ohřevu. Na základě změřeného systematicky nižšího tlaku plynu, i při zohlednění celkové hmotnosti těchto galaxií, usuzujeme, že jejich horké atmosféry mohou být expandující.

Abstract

Many massive elliptical and lenticular galaxies, including those with a significant net angular momentum, are permeated by gas heated to millions of kelvins. Processes shaping the thermodynamic state of the hot gas in non-rotating massive galaxies have been studied over the last few decades. However, the physical properties of rotating hot atmospheres and their connection to colder gas phases have not been investigated systematically. Here, we present a study focused on properties of the hot gas in a sample of fast-rotating lenticular galaxies, observed with the X-ray observatory *XMM-Newton*. In comparison with slow-rotating systems, we measured an enhancement in central entropy and overall flatter radial entropy profiles in rotating galaxies, indicative of relatively higher efficiency of gas-heating in the central regions of these galaxies. We found that the gas pressure in these objects is systemically lower, regardless of the total galaxy mass, and conclude that the hot atmospheres of these objects could be outflowing.



MASARYKOVA UNIVERZITA
Přírodovědecká fakulta

ZADÁNÍ DIPLOMOVÉ PRÁCE

Akademický rok: 2017/2018

Ústav: Ústav teoretické fyziky a astrofyziky

Studentka: Bc. Anna Juráňová

Program: Fyzika

Obor: Teoretická fyzika a astrofyzika

Směr: Astrofyzika

Ředitel Ústavu teoretické fyziky a astrofyziky PŘF MU Vám ve smyslu Studijního a zkušebního řádu MU určuje diplomovou práci s názvem:

Název práce: Systematický výzkum horkých atmosfér obklopujících S0 galaxie

Název práce anglicky: A systematic study of the hot gaseous atmospheres of S0 galaxies

Oficiální zadání:

Massive early type galaxies are known to harbour extended atmospheres of hot X-ray emitting gas. A systematic study of the thermodynamic properties of the hot X-ray emitting haloes has hitherto only been performed for samples of non-rotating giant ellipticals. However, in the presence of significant angular momentum, heating from the central active galactic nuclei (AGN) and radiative cooling are likely to proceed differently. The student will analyse X-ray data for a sample of massive, rotating, S0 galaxies, obtained with the XMM-Newton satellite (and possibly with the Chandra X-ray observatory) and determine the morphology and thermodynamic properties of the hot X-ray emitting atmospheres surrounding these system. The student will compare the properties with those obtained for slow rotating giant elliptical galaxies. The study will inform our understanding of the role of rotation in the formation of cooling instabilities in the process of galaxy formation and evolution.

Jazyk závěrečné práce: angličtina

Vedoucí práce: doc. Mgr. Norbert Werner, Ph.D.

Datum zadání práce: 30. 11. 2017

V Brně dne: 16. 1. 2018

Souhlasím se zadáním (podpis, datum):

.....
Bc. Anna Juráňová
studentka

.....
doc. Mgr. Norbert Werner, Ph.D.
vedoucí práce

.....
prof. Rikard von Unge, Ph.D.
ředitel Ústavu teoretické fyziky a
astrofyziky

Poděkování

My deepest gratitude belongs to my supervisor Norbert Werner for his sincere encouragement, all the invaluable discussions, and patient guidance throughout this work. Besides my supervisor, I would also like to thank Filip Hroch for his generous help and insightful comments, and Kiran Lakhchaura for sharing with me her data. Many thanks belong to my family for their endless support throughout my studies.

Prohlášení

Prohlašuji, že jsem svoji diplomovou práci vypracovala samostatně s využitím informačních zdrojů, které jsou v práci citovány.

Brno, 16. května 2019

Anna Juráňová

Contents

Introduction	ix
1 Hot gas in galaxies	1
1.1 Formation of hot haloes	1
1.2 Influence of AGN	2
1.3 Thermal stability	3
1.4 Warm and cold gas in early-type galaxies	5
1.5 Dynamical state of X-ray atmospheres	7
2 Studied sample	8
2.1 Selection criteria	8
2.2 NGC 3607	10
2.3 NGC 3665	10
2.4 NGC 4382	10
2.5 NGC 4459	11
2.6 NGC 4526	11
2.7 NGC 5353	11
2.8 NGC 1961	12
2.9 NGC 4649	12
3 Data analysis	14
3.1 Observations	14
3.2 Data reduction	15
3.3 Extraction of spectra	16
3.4 Spectral analysis	17
4 Results	19
4.1 Hot gas morphology	19
4.2 Thermodynamic properties	22
4.3 Thermal stability	32
5 Discussion	34
5.1 Hot gas morphology and mass	34
5.2 Thermodynamic properties	36
5.3 Thermal stability	39

6 Summary and conclusions	41
A Supplementary material	42
Bibliography	47

Introduction

During the unending evolution of galaxies, some processes are inevitably hidden from even the most inquisitive human eyes. Particles of gas expelled from stellar atmospheres collide with each other, some of which heat up to form hot haloes that permeate galaxies and even exceed their visible boundaries. In the other direction, from vast and seemingly empty space, gas with a density lower than in ultra-high vacuum falls into galactic gravitational potential wells and heats up to millions of kelvins to glow in X-rays as well. In denser regions of space, the gas is brought also in a more violent manner – during mergers with other galaxies.

But not every galaxy can retain this X-ray emitting atmosphere – the gas can diffuse out of the gravitational potential of the galaxy, it can be stripped off if the host galaxy flies through surrounding medium or it can cool and thus leave energies corresponding to emission of X-ray photons. The cold gas then serves as a source for a formation of new stars or falls onto a central super-massive black hole, which is then capable of launching jets and winds that heat and stir the surrounding medium. A balance between all possible processes changes from galaxy to galaxy, which challenges our understanding of not just the evolution of the hot phase, but galaxies and the Universe as a whole.

It is well-known that spiral galaxies are rotating systems, but the same has been recently measured in many ellipticals and, of course, lenticulars, usually referred to as a transitional type between the former two. Hot atmospheres of galaxies should follow qualitatively same dynamical properties as their stellar components, hence in fast rotating systems, X-ray haloes are subjected to a significant angular momentum. This is expected to affect processes of cooling and heating, apart from being detectable in morphological signatures of the overall motion.

Observations of hot haloes of fast-rotating galaxies are more complicated than those of non-rotating giant ellipticals, which are due to entrapment in deeper potential wells hotter and more luminous. However, the importance of understanding the processes that shape these atmospheres and influence the evolution of their host galaxies lead us to a study of the X-ray emission of rotationally supported galaxies in spite of the practical obstacles.

Hot gas in galaxies

Highly ionized gas confined within gravitational potential wells of galaxy clusters has been successfully studied over last few decades and shed light on behaviour of a supermassive black holes (SMBHs; e.g. Churazov et al., 2005) residing in centres of the brightest cluster galaxies (BCGs), formation of these large-scale objects and the chemical evolution of the Universe (e.g. Mernier et al., 2017). Finely tuned and a rather gentle self-regulation process between the hot halo and an accreting SMBH (active galactic nucleus, AGN), the so-called AGN feedback is becoming less mysterious in these objects. However, in galaxies, where in principle this process is occurring too, its efficiency in retaining hot haloes for billions of years and preventing them from cooling is not well understood (see e.g. Harrison, 2017). In this chapter, we summarize the current understanding of hot atmospheres on galactic scales and expectations resulting from simulations of these objects.

1.1 Formation of hot haloes

During the growth of galaxies on cosmological time-scales, hot gaseous atmospheres were accreted externally and then augmented significantly by stellar mass loss. Today's most massive slow rotating elliptical galaxies are believed to have formed in quick dissipative events lasting a few hundred million years, which produced massive compact galaxies that subsequently grew further in a series of 'dry' (cold gas free) mergers. The fast rotating elliptical and lenticular (denoted S0) galaxies are believed to have formed in 'wet' (gas rich) mergers of spiral galaxies (these merging systems are often called Ultra-Luminous Infrared Galaxies – ULIRGS). Once the mass of the galaxy exceeded approximately $10^{12} M_{\odot}$, the galaxy became surrounded by a hot X-ray emitting atmosphere.

The continuous deepening of the gravitational potential in forming galaxies accelerated clouds of extragalactic gas towards their centres. This externally gained gas was heated to the virial temperature of the galaxy, $T \propto GM/R$. The G here is the gravitational constant, and M and R represent the galaxy mass and radius, respectively. Young stellar populations of star-forming galaxies provided heating and chemical enrichment via stellar winds and – mainly core-collapse – supernovae (SNe), and as the star formation slowed down, heating via stellar explosions became supplied by type Ia SNe. An imprint of these processes, translated to abundances of

heavier elements with transitions at energies in the X-ray band, should in principle be measurable from spectra of the diffuse X-ray emission.

1.2 Influence of AGN

An important role in the evolution of the hot haloes and subsequently the whole galaxies play the central SMBHs, which reside in many massive galaxies and whose past, as well as current, activity is often clearly visible in X-ray observations. These black holes have masses $\gtrsim 10^6 M_\odot$ and processes connected to accretion onto them can be broadly classified as either belonging to radiative or radio/mechanical feedback.

The former one, known also as a quasar mode, is mostly associated with high luminosity AGN as most of the energy is released by radiation. The momentum transfer from radiation to matter then creates outflows of velocity $\sim 10^3 \text{ km s}^{-1}$ which propagate through the galaxy, heating and lowering density of the hot medium and destroying present dust (Morganti, 2017; Barnes et al., 2018; Cielo et al., 2018). Strong radiative feedback requires a high accretion rate onto the SMBH ($\dot{M} \gtrsim 10^{-2} \dot{M}_{\text{Edd}}$), which is not common in present day's ellipticals when radio-mode feedback is dominant in suppressing cooling (Churazov et al., 2005). The Eddington accretion limit is a maximum accretion rate defined for a black hole of mass M_{BH} as $\dot{M}_{\text{Edd}} = 4\pi G m_p M_{\text{BH}} / (\eta c \sigma_T)$. The m_p here is the proton mass, c speed of light, σ_T Thomson cross section, and $\eta = 0.1$ is the radiative efficiency of the accretion process. The limit is given by a balance of the gravitational force and a force associated with radiation pressure, acting in the opposite direction.

The most prominent evidence of radio-mode AGN activity are radio lobes and jets emanating from galactic centres and reaching distances comparable to sizes of the hosting galaxies or larger. The effect of these energetic processes on X-ray atmospheres is directly observable in bubbles devoid of X-ray emitting gas, which reveal themselves as ‘cavities’ of lowered surface brightness in high-resolution X-ray images. These cavities are coincident with radio lobes (where still present) and have been observed in numerous sources, e.g. the BCG of the Perseus cluster (Boehringer et al., 1993) or elliptical galaxy M 84 (Finoguenov and Jones, 2001). Processes involved in the rise of radio bubbles have been found to trigger an uplift of gas from central regions, redistributing colder and metal-rich gas to large distances from the central AGN (Churazov et al., 2001; Simionescu et al., 2008). Similarly, nuclear outbursts are able to produce shocks which propagate through the hot medium and deposit energy into the atmospheres. They are observable as nearly azimuthally symmetric rings or arcs of brightened X-ray emission (Forman et al., 2005). These spectacular manifestations of AGN activity, which are capable of heating the X-ray atmospheres, lead us to a question of the origin of material they ‘feed on’.

The very fact that the hot gas radiates its energy away (and is thus observable) implies cooling of the atmosphere as a whole. In the absence of heating, the atmosphere would cool down and supply material for star formation in a fraction of its age (e.g. Fabian, 1994). Heating provided via AGN and SNe suppresses this catastrophic scenario when the object – an individual galaxy or a galaxy cluster – would cool out

of the X-ray band. However, at certain conditions, the atmosphere is still prone to condensation and subsequently, cooling gas falling to the centre of the potential can fuel the SMBH and trigger an episode of enhanced AGN activity. This, in turn, leads to heating followed by a termination of the cooling phase.

It is critical to note that the feedback mechanism briefly outlined above is not necessarily accurately sustained over large time-scales. This can, for example, happen when the energy contained in jets is deposited beyond the X-ray atmosphere. Observational evidence of this type of unbalanced cooling has been presented by e.g. Grossova et al. (2019).

1.3 Thermal stability

The question of the persistence of X-ray atmospheres has been addressed since the first observations of thermal emission emanating from galaxy clusters and is still a major subject of research in all its aspects. The time required for the hot gas to radiate away its thermal energy, or shortly the cooling time, is here used in the form

$$t_{\text{cool}} = \frac{3(n_e + n_i)k_B T}{2n_e n_i \Lambda(T, Z)}, \quad (1.1)$$

where the electron and ion densities are denoted as n_e and n_i , respectively, and $\Lambda(T)$ stands for the cooling function defined for a given temperature as an emission weighted integral over energy, naturally depending on chemical composition (simplified to metallicity Z) of the gas, which determines the contribution of atomic transitions and overall properties of the gas emission. The form of equation (1.1) comes from its broader definition, i.e. a ratio of gas internal energy, $3/2(n_e + n_i)k_B T$, and its luminosity in unit volume $n_e n_i \Lambda(T, Z)$, but it should be noted that also other definitions are commonly used, employing gas enthalpy in the numerator of (1.1) instead (e.g. Peterson and Fabian, 2006).

This quantity, measurable from spectral properties of the thermal X-ray emission, served as a basis for the ‘cooling flow’ hypothesis (Fabian and Nulsen, 1977; Fabian, 1994). It is based on the assumption that the radiative energy losses of the gas are compensated for by compressional heating as the cooling gas falls to the centre of the gravitational potential. The flow itself would be provided through a decrease in t_{cool} towards smaller radii, caused by an increase in density and a temperature drop. As a result, the gas was expected to flow inwards while cooling, however this scenario has been proven inapplicable to real objects, as expected effects across a wide range of wavelengths are missing or much below theoretical predictions (Peterson et al., 2003). Contrary to the lack of evidence for the uniform global cooling, observations of cold gas, ongoing star formation, and AGN activity in galaxies and clusters require certain amount of gas to cool anyway (e.g. O’Dea et al., 2008; Lakhchaura et al., 2018).

The importance of thermal instabilities in conditions present in hot atmospheres was pointed out even before, by e.g. Field (1965). Thermally unstable gas is prone to development of locally cooling clumps, and in the context of X-ray spectroscopy would lead to formation of a multi-temperature spectrum. Conditions under which the thermal instabilities can develop from perturbations in the hot plasma and grow

non-linear depend on effectiveness of thermal conduction, viscosity and magnetic fields (McCourt et al., 2011), and a prevalence of turbulent mixing (Scannapieco and Brüggén, 2008) and heating (Zhuravleva et al., 2014).

Rees and Ostriker (1977) suggested that the ratio of the cooling time (1.1) and the gravitational free-fall time, defined for a given radius r and gravitational acceleration g simply as

$$t_{\text{ff}} = \sqrt{\frac{2r}{g}}, \quad (1.2)$$

is a crucial quantity in determining whether the gas is thermally stable or not. They argued that radiatively cooling pressure-supported clouds can re-adjust quasi-statically and prevent a rapid cooling to temperatures of 10^4 K, as long as the cooling time exceeds the free-fall time. In the opposite case, over-dense blobs, formed through local non-linear perturbations in the hot medium, are expected to disconnect from the hot phase and fall onto the AGN, as depicted in Pizzolato and Soker (2005), provided they are prevented from evaporation by thermal conduction.

With the advance of numerical simulations, this picture has been revisited and modified by Sharma et al. (2012), who concluded that thermal instabilities develop from linear perturbations and produce multiphase gas when the value of $t_{\text{cool}}/t_{\text{ff}}$ falls below approximately ten. Observationally, galaxies with ongoing cooling, and thus having this ratio below the suggested threshold, are expected to produce detectable emission from colder phases of atomic and molecular gas. Evidence for the validity of this criterion has been presented for many systems, yet it does not seem to be universally consistent with observations, as e.g. only 10 of 43 galaxy clusters studied in Voit and Donahue (2015) with detectable H α emission have a minimum of measured $t_{\text{cool}}/t_{\text{ff}} < 10$, similarly in Hogan et al. (2017).

Generally, hot haloes do not seem to fall much below the $t_{\text{cool}}/t_{\text{ff}} \approx 10$ threshold, on scales of galaxies to galaxy clusters, as recently summarized in Voit et al. (2018). Combining previously published results for a number of objects (individual ellipticals, groups and clusters), they concluded that processes operating in hot atmospheres are regulated so that they hold onto this ratio as a lower limit over seven orders of magnitude in X-ray luminosity. Additionally, in a sample of 96 early-type galaxies (ellipticals or lenticulars, denoted ETGs), Babyk et al. (2018c) found no connection of $t_{\text{cool}}/t_{\text{ff}}$ ratio and a presence or absence of observable cold gas. The cooling time alone, on the contrary, seems to be closely connected to molecular gas content. Pulido et al. (2018) and Babyk et al. (2018c) find a cooling time threshold of $t_{\text{cool}} < 1$ Gyr for its presence in ETGs.

Striving to explain the processes of condensation from hot haloes, scenarios leading to a formation of observed cold gas structures have been proposed over time. Numerical simulations of cooling in hot atmospheres, which predict sufficient feeding of the central SMBH, have been performed by Gaspari and Churazov (2013). Subsonic turbulent motions (originated in e.g. AGN activity or mergers, with velocity dispersion $\sigma_v \sim 150 \text{ km s}^{-1}$) in their models significantly alter the process of condensation, inducing chaotic gas dynamics, due to which perturbations become non-linear and

form multiphase filaments detectable in longer wavelengths. This ‘chaotic cold accretion’ (CCA) and its direct connection to AGN heating should be capable of stabilising the hot atmosphere at $t_{\text{cool}}/t_{\text{ff}} \approx 10$.

Li et al. (2015) predicted from their numerical simulations (omitting magnetic fields and thermal conduction) that condensation should develop from gas uplifted by AGN-triggered jets from its initial equilibrium position. The precipitation itself should then proceed via interaction with the jet. Similar results in terms of the influence of jets were presented by Prasad et al. (2015), who used a different approach in numerical simulations. This ‘stimulated feedback’, in which the precipitation from hot phase is observed due to uplift from central regions, has been supported observationally in several objects (McNamara et al., 2016; Tremblay et al., 2018).

The state of a hot atmosphere with respect to ongoing cooling has been recently claimed to be given more accurately by a different dimensionless parameter than $t_{\text{cool}}/t_{\text{ff}}$ (Gaspari et al., 2018). Condensation via CCA, related to density-fluctuations driven by turbulence, should be present in conditions where turbulent time-scale (t_{eddy} defined below) is comparable to cooling time-scale, set by the proposed C -ratio

$$C \equiv \frac{t_{\text{cool}}}{t_{\text{eddy}}} \approx 1. \quad (1.3)$$

The time required for a gyration of individual turbulent eddies, or the eddy turnover time, is defined as

$$t_{\text{eddy}} = 2\pi \frac{r^{2/3} L^{1/3}}{\sigma_{v,L}}, \quad (1.4)$$

where $\sigma_{v,L}$ is the velocity dispersion at the injection scale length L , consistent with a diameter of the cold/warm gas. The velocity dispersion is not easily measurable even in high-resolution X-ray spectra, but it can be obtained from measurements of motions in products of the cooling process, the cold/warm gas.

1.4 Warm and cold gas in early-type galaxies

Regardless of the exact mechanism, cooling from X-ray phase should naturally lead to a presence of gas at lower temperatures, observable in longer wavelengths. Warm ($T \sim 10^4$ K) gas, bright in optical $\text{H}\alpha + [\text{N II}]$ lines, is commonly observed in regions associated with ongoing star formation, where the UV emission of young stars ionizes the surrounding gas. However, the warm gas has also been observed in galaxies and galaxy clusters where the star-formation rate is not sufficient to warm the nearby cold gas and the correlation between ionizing UV emission and $\text{H}\alpha$ has been found to be weak and with a large scatter (McDonald et al., 2010). Supporting the evidence for condensation from the hot phase, presence of $\text{H}\alpha$ filaments has been found to strongly correlate with other properties suggesting a cooling of X-ray atmosphere (e.g. McDonald et al., 2011).

These measurements are commonly performed with narrow-band filters or spectroscopically, where N II lines at 6548 Å and 6583 Å are blended with the 6563 Å $\text{H}\alpha$ line.

In an analysis of 147 ETGs selected from volume-limited survey ATLAS^{3D} for having available data, 37% were detected in H α (Gavazzi et al., 2018).

Atomic hydrogen can be directly observed at wavelength $\lambda = 21.11$ cm (or frequency of $\nu = 1.4$ GHz) thanks to the hyperfine splitting of the electronic ground state of H I (Draine, 2011, pg. 70). Simulations of Lagos et al. (2014) predict that early-type galaxies acquire their atomic gas from radiative cooling of hot atmospheres and, in smaller amounts, through minor mergers or directly from the stellar mass loss. Studying H I emission in early-type galaxies, Lucero and Young (2013) found comparable kinematic properties of atomic hydrogen and molecular gas, consistent with a common origin of the two phases. Cold gas at temperatures $T \sim 100$ K can be observable in far infra-red (FIR) spectra via forbidden lines [C II] $\lambda 157 \mu\text{m}$, [O I] $\lambda 63 \mu\text{m}$ and [O IB] $\lambda 145 \mu\text{m}$ (Ferland et al., 1994). These emission lines have been observed in e.g. filamentary emission nebula of multiphase gas likely uplifted by an AGN in M87 galaxy (Werner et al., 2013).

Even though the molecular hydrogen is the most abundant molecule in cold molecular gas ($T \lesssim 50$ K) in galaxies, it has no observable transitions equivalent to temperatures that low and is therefore not directly observable. Instead, the second most abundant molecule, CO, which has a permanent dipole moment, serves as a common tracer of molecular gas. Observations of its transition between states with rotational quantum number $J = 1$ to $J = 0$, CO($J = 1 \rightarrow 0$), at 2.6 mm have been established as a useful tool for the total molecular hydrogen mass estimate, via CO luminosity to H₂ mass conversion, in which $N(\text{H}_2)/I(1 \rightarrow 0) = 3 \times 10^{20} \text{ cm}^{-2} (\text{K km s}^{-1})^{-1}$ (Dickman et al., 1986). Transitions between higher rotational states CO($J = 2 \rightarrow 1$) at 1.3 mm, CO($J = 3 \rightarrow 2$) at 0.87 mm trace gas at increasingly higher temperatures and densities (e.g. Neininger et al., 1998; Harris et al., 2010). Cold molecular gas in BCGs is most probably a result of cooling from the hot intracluster medium, predicted from the theoretical side and also observed near centres of clusters in a form of thin filaments with lengths on kiloparsec scale (Bridges and Irwin, 1998; Conselice et al., 2001). In less massive and smaller systems, groups and isolated galaxies, the issue is more complex, allowing other processes to come into play. Recent surveys focusing on CO emission in early-type galaxies, SAURON, ATLAS^{3D} and MASSIVE found the presence of molecular gas in 28% (12/43 galaxies; Combes et al., 2007), 22% (56/259 galaxies; Young et al., 2011) and 25% (17/67 galaxies; Davis et al., 2019), respectively, of studied objects. For the ATLAS^{3D} sample, Young et al. (2011) found no correlation with stellar (K-band) luminosity, which implies that the molecular gas does not originate purely in stellar mass loss. Total galaxy masses in their sample are not all above the threshold for retaining hot haloes and therefore for those the origin in condensation from hot atmospheres can be ruled out. However, in ETGs massive enough to host hot atmospheres, Babyk et al. (2018c) found a correlation between mass X-ray halo and molecular hydrogen content. The H₂ was reported to be in systems with t_{cool} as short as 10^9 yr, indicating a condensation from hot atmospheres.

Apart from a gas of various properties, dust and polycyclic aromatic hydrocarbons (PAHs) are observed in massive ETGs with cold gas in their centres, ranging from BCGs to solitary galaxies (Donahue et al., 2011; Kokusho et al., 2017). PAHs are produced in winds of evolved stars, just as the dust, and are generally easily destroyed by X-rays

and hard UV photons. Hence, they are expected to be present in dense regions together with dust and shielded by layers of X-ray absorbing medium (Monfredini et al., 2018).

1.5 Dynamical state of X-ray atmospheres

In the general absence of strong cooling flows, hot atmospheres in isolated ETGs are usually assumed to be in or close to hydrostatic equilibrium. However, if the global gas heating exceeds the radiative cooling, the atmosphere could change from stable to out-flowing state. Pellegrini (2012) showed in her work that the energy injection through SNe at a given time, a function of stellar luminosity of the galaxy, becomes dominant for low luminosity systems (with $L_B \lesssim 3 \times 10^{10} L_{B,\odot}$ derived for properties of early-type galaxies determined from usual scaling relations and for low redshift galaxies, see Pellegrini, 2012, for more details). Although other processes influencing the thermodynamic state of the hot gas operate in galaxies too, this threshold suggests that outflows are likely present in low-mass systems and can have a significant effect on properties of X-ray haloes. Furthermore, the dynamical state of the central region can be decoupled from gas at larger radii, due to which only partial outflow (or inflow) could be present.

Observations of *Einstein* observatory revealed that the X-ray luminosity L_X of early-type galaxies is related to its stellar shape. Derived ratios of L_X/L_B (thus independent of stellar mass) for pure ellipticals were found to be systematically higher than those of ‘discy’ ellipticals and S0s (Eskridge et al., 1995). The flattened shape of the gravitational potential and rotational support, which has been confirmed for flattened ETGs (Emsellem et al., 2011), should allow easier development of outflows.

From the view of thermal stability, Juráňová et al. (2019) found spectral features indicating ongoing cooling in the plane of rotation of a lenticular galaxy NGC 7049 which has a multiphase disc ranging from warm gas to cold molecular phase. The spectra extracted from regions in the perpendicular direction, where the gas should be supported only by buoyant force, were found to be consistent with single temperature gas. These findings have been attributed to effects of rotation, where the thermally unstable clumps of gas subjected to significant angular momentum are effectively slowed down in radial direction and therefore prevented from reaching equilibrium position. This scenario has also been proposed from numerical simulations of Gaspari et al. (2017), where the CCA in rotationally supported hot atmospheres should proceed differently. In the case where rotation is the dominant motion in the hot gas, i.e. where the rotational velocity v_{rot} exceeds the velocity dispersion σ_v (as in NGC 7049), described by the so-called turbulent Taylor number $\text{Ta}_t \equiv v_{\text{rot}}/\sigma_v > 1$, the condensation should proceed along helical paths and lead to a creation of a multiphase disc.

Studied sample

2.1 Selection criteria

To study the properties of the hot gas in rotating lenticular galaxies, we selected our objects based on several criteria. Given its origin, the gas motion can be probed by that of the galaxy's stellar component, which we therefore used for a selection of galaxies whose hot atmospheres are rotationally supported. The recent extensive study of the kinematics of early-type galaxies, the ATLAS^{3D} Project (Cappellari et al., 2011), provides an excellent basis for this selection, as among the main results are the 2D maps of stellar velocities measured along the line of sight.

Moreover, all the objects in their sample have distances below 42 Mpc, which makes them satisfy a straightforward requirement on sufficient proximity, which would allow us to perform a spatially resolved analysis of their extended X-ray emitting atmospheres.

Taking into account the expected properties of the observed X-ray sources and the main objectives of this work, we decided to use archival data from the X-ray space observatory *XMM-Newton* (X-ray Multi-Mirror Mission, Jansen et al., 2001). Compared to other X-ray telescopes with a spatial resolution needed in our case, the instruments onboard of this spacecraft are sensitive in energies below 1 keV. This is a crucial quality for observations of S0 galaxies, as the temperature of the gas scales with the total mass of the galaxy, which is in S0s generally lower than in giant ellipticals commonly observed in X-rays. This narrowed down the sample to six galaxies, introduced in detail in the following sections, followed by two more objects: a spiral galaxy with a hot halo – NGC 1961, and an elliptical galaxy NGC 4649, which is, according to findings in ATLAS^{3D} Project, also rotationally supported. Optical images of the whole sample are shown in Fig. 2.1.

In the following sections, the studied objects are presented, focusing on properties related to AGN and stellar feedback. Table 2.1 and Table 2.2 provide a quantitative characterisation of properties relevant for this study, some of which were collected using the NASA/IPAC Extragalactic Database¹.

¹The NASA/IPAC Extragalactic Database (NED) is operated by the Jet Propulsion Laboratory, California Institute of Technology, under contract with the National Aeronautics and Space Administration.

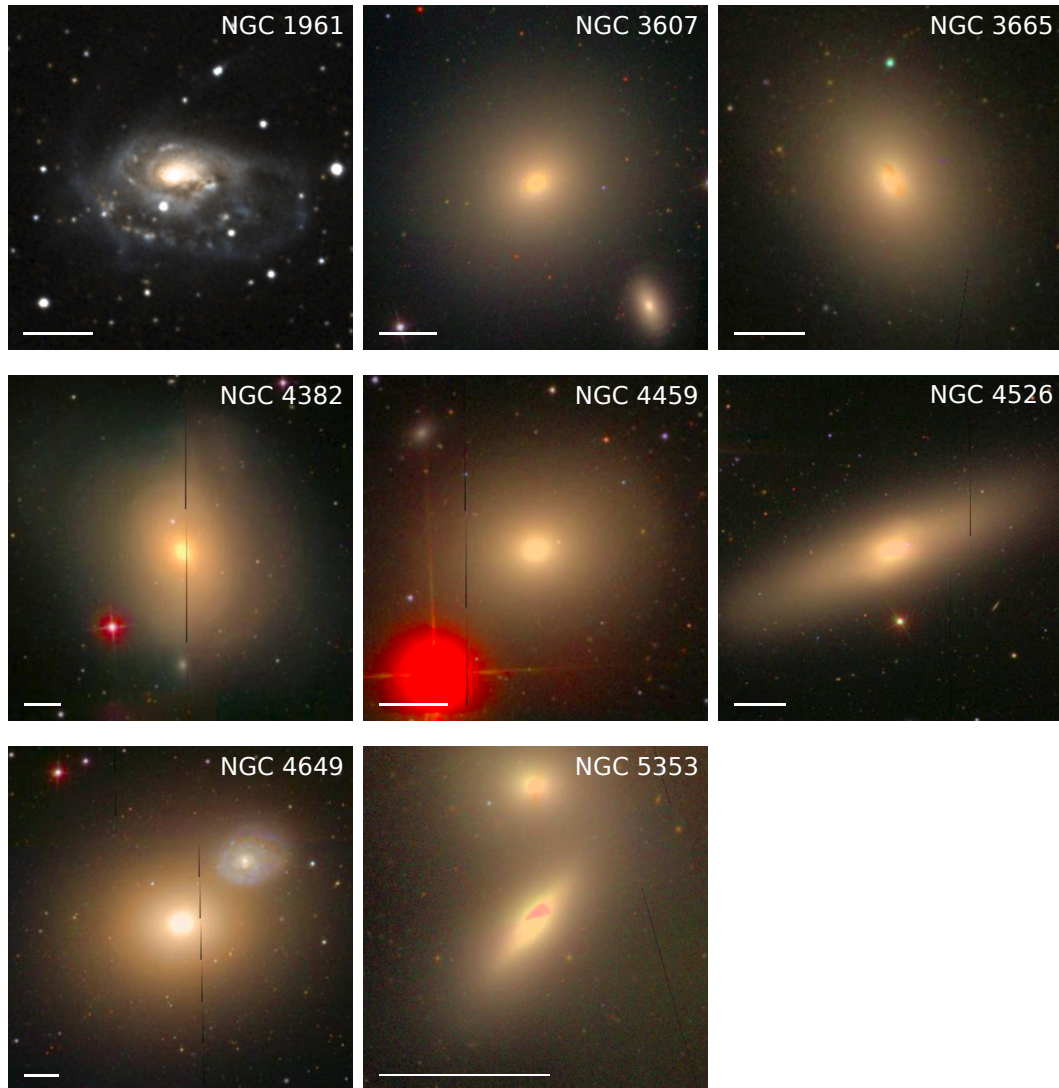


Figure 2.1: Optical images of the studied sample of S0 galaxies, NGC 1961 and NGC 4649. The images are taken from Sloan Digital Sky Survey (SDSS, data release 7) with an exception of NGC 1961, which is from Digitalised Sky Survey 2. The solid line in the lower-left corner of every image represents a scale of 1 arcmin.

2.2 NGC 3607

NGC 3607 is an unbarred lenticular galaxy (morphological type SA0) and the brightest member of Leo II group, and according to Giuricin et al. (2000) it is accompanied by another 18 galaxies. It has the highest SFR in our sample, $0.42 M_{\odot} \text{yr}^{-1}$. From measurements of globular clusters kinematics, Alabi et al. (2017) found that within five effective radii, dark matter contributes to the total enclosed mass in this galaxy only by $\sim 16\%$, which is by a factor of 3 lower than in other non-BCGs early-type galaxies and what is predicted from cosmological hydrodynamical simulations. What Alabi et al. propose as an explanation for this discrepancy is that the galaxy formed much later on cosmological time-scales than most of the early-type galaxies. *Chandra X-ray Observatory* measurements do not show evidence for an X-ray bright AGN.

2.3 NGC 3665

Another SA0 type galaxy in our sample, NGC 3665, is the brightest member of a group of 11 galaxies (Makarov and Karachentsev, 2011). It has the highest luminosity from the emission of polycyclic aromatic hydrocarbons, triggered by absorption of far-ultraviolet light, for which it can be used as a tracer of ongoing star formation. However, the star-formation rate measured by other methods is in this system still relatively low $\sim 0.1 M_{\odot} \text{yr}^{-1}$. NGC 3665 is among our radio brightest S0s at 1.4 GHz and is the only one in our sample that shows a pronounced radio activity associated with an AGN. Twin jets were observed by Very Large Array (Parma et al., 1986), and core radio emission obtained from very-large-array interferometry at 5 GHz (Liuzzo et al., 2009). The mass of the supermassive black hole was measured by Onishi et al. (2017) to be $M_{\bullet} = 5.8 \times 10^8 M_{\odot}$.

2.4 NGC 4382

This object, known also as M 85, resides in the Virgo cluster and it is the only galaxy in our sample, which does not have a disc of cold gas near its centre. The morphological type of this galaxy is SA0 again, but this time, the galaxy also shows shell-like structures. These features are believed to form from in-falling smaller galaxies that oscillate in the gravitational-potential well and form arcs of stars expanding to the outskirts of the galaxy (see e.g. Thomson, 1991). The lack of cold gas is consistent with observed low star formation, $0.002 M_{\odot} \text{yr}^{-1}$.

Capetti et al. (2009) found that the core of NGC 4382 does not show any radio emission related to a central black hole, which is highly unusual for such a large early-type galaxy. More recently, Gültekin et al. (2011) presented results from measurements of stellar kinematics in the centre of NGC 4382 observed by Hubble Space Telescope, which suggest that this galaxy may indeed not have a SMBH. More precisely, the current black hole mass scaling relations, $M_{\bullet} - L$ (Kormendy, 1993) and $M_{\bullet} - \sigma$ (Ferrarese and Merritt, 2000; Gebhardt et al., 2000), predict a significantly larger black hole mass when compared to their best-fitting value $M_{\bullet} = 1.3 \times 10^7 M_{\odot}$, a result consistent with an anomalously low-mass black hole, if present. This result, along

with no signs of past AGN activity, suggests that the observed X-ray halo could be maintained purely by stellar feedback.

2.5 NGC 4459

Another member of the Virgo cluster, NGC 4459, is an unbarred lenticular galaxy with a dusty disc extending out to $r \sim 0.7$ kpc, with observed blue clumps suggesting a presence of newborn stars (Ferrarese et al., 2006). Unable to detect any neutral hydrogen in their observations, Lucero and Young (2013) provide only an upper limit on its mass, $M_{\text{HI}} < 1.7 \times 10^7 M_{\odot}$, despite the well measurable presence of molecular hydrogen (see Table 2.2), yielding ratio $M_{\text{H}_2}/M_{\text{HI}} > 21$. Far- and mid-infrared emission of gas was studied in detail by Young et al. (2009) and led to a detection of $24\mu\text{m}$ emission from a disc reaching out to $r \sim 2.6$ kpc, which exceeds almost four times the radius of the dusty structures and thus cannot be attributed to ongoing star formation. They also find that NGC 4459 has the so-called FIR-excess, i.e. FIR-to-radio flux density ratio exceeding a value of 3.04, a rare feature defined from observations of a large sample of galaxies in Yun et al. (2001). In the centre of NGC 4459, Gavazzi et al. (2018) report detection of $\text{H}\alpha$ emission. An X-ray image from *Chandra* revealed a point source co-spatial with the centre of the galaxy, and another point source separated by ~ 4.5 arcsec from the first one.

2.6 NGC 4526

The only barred lenticular galaxy (SAB) in our sample, NGC 4526, is also a member of the Virgo Cluster. Having two occurrences in the New General Catalogue, it is also known as NGC 4560. Hereafter, we will only use the designation NGC 4526 for this object, which is also preferred in the scientific community. It is oriented nearly edge-on and also possesses a dusty disc in the plane of rotation, spanning over central $r \sim 1.2$ kpc. Star-formation rate is in NGC 4526 the smallest among galaxies with a dusty disc in our sample and the PAH luminosity the second highest, $\sim 17 \times 10^{41} \text{ W Hz}^{-1}$. As in the case of NGC 4459, Lucero and Young (2013) did not detect neutral hydrogen and only put an upper limit onto the $M_{\text{HI}} < 1.9 \times 10^7 M_{\odot}$, while the total mass of present H_2 was measured well (see Table 2.2). The lower limit of their ratio is thus even larger than in NGC 4459: $M_{\text{H}_2}/M_{\text{HI}} > 100$. Focusing on the warm gas content, Gavazzi et al. (2018) found $\text{H}\alpha$ emission with a disc-like morphology in this galaxy. Davis et al. (2013) measured the mass of the central supermassive black hole to be $M_{\bullet} = 4.5 \times 10^8 M_{\odot}$.

2.7 NGC 5353

This almost edge-on oriented galaxy is a member of HCG 68 compact group with NGC 5350 and NGC 5354 and two more objects (Hickson, 1982), accompanied by other 45 fainter galaxies and more member candidates (Tully and Trentham, 2008). It has an effective radius of only ~ 3.4 kpc, which is smaller than any of the other 5

lenticular galaxies in this study. O’Sullivan et al. (2018) found a CO disc with a radius of 0.8 kpc and also a dusty disc in the central $r \sim 0.5$ kpc was observed (Goullaud et al., 2018). Its rotational velocity is very close to the velocity dispersion, which makes this galaxy a great example of the transition between rotation-dominated galaxies and slow rotators. This object is classified as a LINER (low-ionization nuclear emission-line region) galaxy (e.g. Saikia et al., 2018). Sánchez-Sutil et al. (2006) reported an X-ray bright nuclear point source emission spatially coincident with a radio source, which can be associated with a central AGN. Finoguenov et al. (2007) studied the hot intragroup medium of HCG 68, finding the temperature of the gas in two radial bins from the centre of the group: $k_{\text{B}}T(< 31 \text{ kpc}) \approx 0.66 \text{ keV}$ and $k_{\text{B}}T(< 92 \text{ kpc}) \approx 0.69 \text{ keV}$ with overall metallicity measured only in the inner one, $Z = (0.18 \pm 0.04) Z_{\odot}$.

2.8 NGC 1961

This rotation-dominated spiral galaxy is the brightest member of a small group of seven galaxies (Tempel et al., 2016) and it has been classified as a LINER galaxy (Carrillo et al., 1999). Measurements of rotational velocity at distances exceeding 10 kpc from the galaxy centre (Rubin et al., 1979) have revealed that this spiral galaxy is exceptionally massive, and at the same time, X-ray observations showing a point source located in the centre of the galaxy confirm a presence of an AGN. The total mass of the galaxy is more than sufficient to retain its hot gaseous halo, which has been observed by both *Chandra* and *XMM-Newton*. Bogdán et al. (2013) compared available observations of NGC 1961 with results from numerical simulations finding that the galaxy is dark matter dominated – baryons contribute to the total mass with only 11 %. In radio observations at 6 and 18 cm presented in Krips et al. (2007), nuclear emission is accompanied by a $\sim 2\sigma$ signal resembling radio jets. Additionally, distorted HI morphology revealed that the gas is being stripped by the surrounding intragroup medium (Shostak et al., 1982).

2.9 NGC 4649

This elliptical galaxy, also known as M 60, resides in a group within the Virgo Cluster (Mamon, 2008). Traces of motion of the galaxy with respect to the parent cluster are pronounced in the disturbed shape of its X-ray atmosphere, where ram-pressure stripping and Kelvin-Helmholtz instabilities driven by the interaction of the hot atmosphere of NGC 4649 and the intra-cluster medium were clearly observed (Wood et al., 2017). Another deviation from the spherical symmetry, this time closer to the galaxy centre, is connected to the AGN activity, as radio-jets inflated cavities in the X-ray gas can be observed in images from *Chandra* and are presented in e.g. Shurkin et al. (2008); Dunn et al. (2010). This galaxy does not have clearly observable dusty features, which is supported by no FIR emission detections reported by Temi et al. (2003).

In ATLAS^{3D} Project, this galaxy is also classified as a fast rotator, but close to the slow-/fast-rotator classification threshold. The support in the X-ray gas atmosphere

created by its rotation is negligible relative to the gas pressure support.

Table 2.1: Basic observational properties of the studied sample. Distance d is adopted from ATLAS^{3D} Project and references therein with the exception of NGC 1961, in which case the median value of distances from NED was taken, as well as values for redshift (z) in the second column. The effective radii R_e , velocity dispersions and rotational velocities are adopted from Cappellari et al. (2011).

object NGC	d Mpc	z 10^{-3}	scale arcsec kpc ⁻¹	R_e arcsec	σ_v km s ⁻¹	v_{rot} km s ⁻¹
3607	22.2	3.14	9.29	38.9	222.0 ± 4.0	110.0 ± 9.0
3665	33.1	6.90	6.23	30.9	215.0 ± 8.5	94.3 ± 21.5
4382	17.9	2.43	11.52	66.1	68.3 ± 16.5	176.0 ± 3.5
4459	16.1	3.98	12.81	36.3	75.0 ± 20.0	171.8 ± 4.8
4526	16.4	2.06	12.58	44.7	150.4 ± 8.6	246.0 ± 6.0
5353	35.2	7.75	5.86	20.0	298.0 ± 9.0	284.0 ± 4.8
1961	32.4	13.12	6.37	51.0	242.0 ± 12.0	326.8 ± 9.5
4649	17.3	3.70	11.92	66.1	330.5 ± 4.6	55.0 ± 22.1

Table 2.2: Observational properties of the composition of the sample galaxies. B -band stellar luminosity L_B and $B-V$ colour index are taken from HyperLEDA (Makarov et al., 2014), 1.4 GHz radio power from Brown et al. (2011) and Condon et al. (2002), PAH luminosity from Kokusho et al. (2017) and Stierwalt et al. (2014) in the case of NGC 1961, mass of molecular hydrogen Young et al. (2011) and Combes et al. (2009) for NGC 1961, mass of atomic hydrogen from Young et al. (2014) and Haan et al. (2008) for NGC 1961. PAH luminosity has not been constrained for NGC 4649, just as atomic hydrogen content in NGC 4382 and NGC 4526.

object NGC	L_B $10^{10} L_{B,\odot}$	$B-V$ mag	$\log P_{\text{radio}}$ W Hz ⁻¹	L_{PAH} 10^{41} erg s ⁻¹	$\log M_{\text{H}_2}$ M_{\odot}	$\log M_{\text{HI}}$ M_{\odot}	SFR $M_{\odot} \text{ yr}^{-1}$
3607	3.70	0.93	20.63	7.8 ± 6.2	8.42	< 6.53	0.420
3665	3.37	0.93	22.04	45.1 ± 9.9	8.91	< 7.05	0.109
4382	5.86	0.89	< 19.79	0.3 ± 5.5	< 7.39	–	0.002
4459	1.45	0.97	< 19.63	7.1 ± 2.9	8.24	< 6.53	0.071
4526	2.42	0.98	20.61	17.1 ± 4.4	8.59	–	0.028
5353	3.56	1.03	21.62	2.3 ± 6.7	< 7.44	< 7.07	0.095
1961	22.91	0.86	22.82	37.8 ± 3.1	10.39	10.67	9.24
4649	6.19	1.00	20.97	–	< 7.44	< 7.19	0.129

Data analysis

3.1 Observations

Instruments which collected the data we use in our analysis are named collectively as European Photon Imaging Camera (EPIC), each lying in the focal plane of one of the three X-ray telescopes onboard *XMM-Newton* X-ray observatory. Each of these detectors covers a field of view 30 arcmin (Jansen et al., 2001) and has a useful quantum efficiency at 0.2 – 10 keV.

The EPIC-pn camera consists of an array of 12 CCD chips which operate in parallel. The observations we use were performed in a full frame or extended full frame operating mode, with the active detector area covering the whole field of view. In the full frame mode, each of the CCD subunits has an integration time of 68.7 ms followed by 4.6 ms readout. Extended full frame mode has longer integration time, 199.2 ms, and the same readout time (Strüder et al., 2001). Photons detected during the readout period (6.3 % in full frame and 2.3 % in extended full frame mode of the observation time) are assigned to a wrong position and need to be accounted for properly during the data analysis. The angular resolution of *XMM-Newton* is 15 arcsec half energy width at 1.5 keV and thus much larger than the size of EPIC-pn pixels (4.1 arcsec side). The energy resolution at 1.5 keV is ~ 110 eV (full width at half maximum, FWHM) and ~ 150 eV (FWHM) around 6 keV (Strüder et al., 2001).

Remaining two EPIC instruments, EPIC-MOS, are assembled of 7 MOS-type CCDs each, some of which have been lost over time due to micrometeorite hits. Only 44 % of the total flux reaches the detectors as half of the arriving photons are diverted to reflection grating spectrometers. This allows a longer integration time, which is 2.6 s and available continuously. One pixel covers only 1.1×1.1 arcsec and the energy resolution at 1.5 keV is also better than in EPIC-pn, ~ 80 eV (FWHM), but at 6 keV, the resolution decreases to ~ 150 eV (FWHM) as well (Turner et al., 2001). Positions of individual CCDs of all EPIC instruments are designed to overlap in a way that the detector chip gaps are mutually covered, in principle resulting in an image of the whole field of view.

For the analysis described below, we used all EPIC observations with any useful exposure time available at *XMM-Newton* Data Archive. These observations, denoted by an observation ID (OBSID), are listed in Table 3.1. In *XMM-Newton* EPIC observations, each event (i.e. a detection on a CCD chip) is stored with information on energy, detection time and position on the chip. This allows subsequent filtering of

Table 3.1: List of used observations for each galaxy and exposure times. In the second column, observation ID is given, for which the total observation time t_{tot} in MOS1, MOS2 and pn detectors is shown in columns 3, 4, and 5, respectively, and the useful exposure time t_{net} (not contaminated by soft-proton flaring) is written in the next 3 columns. The sum of the flaring-excluded exposure time in all instruments together is given in the last column.

object	OBSID	t_{tot} [ks]			t_{net} [ks]			$\sum t_{\text{net}}$ [ks]
		M1	M2	pn	M1	M2	pn	
NGC 1961	0673170101	31.5	31.5	30.4	21.5	23.5	11.3	
	0673170301	35.0	35.1	34.0	21.2	21.1	17.5	
	0723180101	21.8	21.8	20.8	19.8	19.6	15.9	
	0723180201	21.6	21.5	19.9	11.9	10.6	3.0	
	0723180301	23.9	23.8	22.7	16.3	18.1	9.3	
	0723180401	18.6	18.8	20.7	7.1	6.6	3.3	
	0723180601	25.6	25.5	23.9	9.1	9.8	7.0	
	0723180701	20.9	20.8	19.2	7.3	7.5	5.5	
	0723180801	14.7	14.6	19.0	13.6	13.6	9.7	
0723180901	23.2	23.1	21.5	13.2	13.7	8.9	376.7	
NGC 3607	0099030101	22.3	22.3	20.0	15.6	17.6	10.8	
	0693300101	44.4	44.4	43.8	31.3	35.3	19.8	130.4
NGC 3665	0052140201	40.6	40.6	36.3	27.8	29.6	20.3	77.6
NGC 4382	0201670101	33.5	33.5	33.2	18.8	18.8	14.4	
	0651910401	41.7	41.6	40.6	33.6	34.1	25.7	
	0651910501	41.2	41.3	40.2	29.9	29.6	24.1	
	0651910601	41.2	41.1	40.1	27.7	28.7	22.1	
	0651910701	36.5	36.5	34.9	28.3	28.3	24.2	388.3
NGC 4459	0550540101	81.8	81.8	82.8	72.7	73.2	60.6	
	0550540201	20.4	20.4	18.8	18.8	18.8	15.1	259.1
NGC 4526	0205010201	25.9	25.9	26.0	22.0	21.9	17.7	61.6
NGC 4649	0021540201	51.3	51.3	49.0	49.0	48.2	38.9	
	0502160101	81.7	81.7	80.5	72.9	72.7	61.0	342.6
NGC 5353	0041180401	22.3	22.3	20.0	21.3	21.1	16.8	59.1

events unrelated to the observation target, which is described below.

3.2 Data reduction

The data were reduced with standard procedures of *XMM-Newton* Science Analysis System version 17.0.0. Event lists from raw-data files were obtained using tasks `emchain` for EPIC-MOS and `epchain` in the case of EPIC-pn. Prior to filtering of the output datasets, we also created a model of events received at times of relatively long

readout of pn (the so-called out-of-time events). For this step, `epchain` task was run for a second time with a corresponding option to obtain an observation-specific event list (hereafter OOT-event list), which was, after proper scaling, subtracted from the pn event list.

Almost every observation of *XMM-Newton* is contaminated by events triggered in collisions of highly energetic protons with the detectors. These particles with energies comparable to X-ray photons, focused by *XMM-Newton* optics and often referred to as soft protons, originate in Solar activity and are trapped in Earth’s magnetosphere which is crossed by *XMM-Newton* during every revolution. In times of the highest soft-proton (SP) flaring, the telescope is not operating to prevent permanent damage to the detectors, but minor flares can be witnessed any time (Jansen et al., 2001). The spectral profile of the SP component varies in time and is thus impossible to be accounted for during the spectral analysis. Fortunately, periods of anomalously high noise due to SP contamination can be defined and excluded from event lists based on a light curve of individual observations. The SP unaffected times (good time intervals, GTI) in our observations were determined based on a count-rate threshold set manually from light curves observed at energies from 10 to 12 keV, which is a commonly used approach in this situation. The total and reduced exposure times resulting from the GTI cleaning, t_{tot} and t_{net} , respectively, are given in Table 3.1 to illustrate the quality of the data used further on.

The event files were then filtered omitting detections flagged as unreliable, following standard processing recommendations¹. When an X-ray photon hits the detector, it creates a geometrical pattern of pixels where any signal was detected. We excluded all events unsatisfying a condition `PATTERN<=12` for MOS1, MOS2 which leaves out larger than ‘quadruple’ patterns, and `PATTERN<=4` for pn, resulting in a use of patterns quoted only as ‘single’ or ‘double’. Events excluded by these inequalities cannot be attributed to genuine X-ray photons and would pollute the observation if used. In addition to these criteria, recommended strings `#XMMEA_EM` and `#XMMEA_EP && (FLAG==0)` were used for filtering of EPIC-MOS and EPIC-pn event files, respectively, to apply further corrections.

3.3 Extraction of spectra

To study the X-ray emitting gas in every galaxy presented in Chapter 2, we extracted spectra from several concentric annuli, which allowed us to create radial profiles of derived physical properties. Of course, this can be done only with the assumption of spherical symmetry (azimuthal in projection), which will be discussed in the following chapters. Where the number of received photons allowed it, we used the highest reasonable spatial resolution, where the width of each annulus is given by the angular resolution of *XMM-Newton*. This was unfortunately not the case of a majority of galaxies in our sample, where the span of each annulus was determined by a number of counts in a selection region that led to a reliable spectral analysis.

¹XMM-Newton Users Handbook, Issue 2.16, 2018 (ESA: XMM-Newton SOC, 2018)

Typically, X-ray point sources of various origin are projected onto the extended emission of interest. To avoid their undesired contribution to the spectra, we encircled the emission of each point source and excluded the selected events during the spectral extraction procedure.

As none of the X-ray atmospheres of interest covered the entire field of view, it was possible to create a spectrum of local background to be subtracted prior to spectral analysis. This approach to the handling of remaining events unrelated to the examined source is based on the reasonable assumption that the background spectrum is representative of the true background of the studied spectrum. Having the brightest point sources removed by hand, the remaining contamination by distant AGNs does not vary considerably. This also applies to diffuse soft X-ray foreground, which changes at much larger spatial scales compared to the *XMM-Newton* field of view. Another possible treatment is based on a modelling of all background components and thus requires further assumptions on their spectral properties and, at the same time, the sufficiently high number of received background photons to reliably constrain their parameters.

3.4 Spectral analysis

A spectrum of a million-kelvin plasma in our galaxies is determined primarily by the temperature of the gas, its density and abundances of present elements. For the spectral fitting, we used the SPEctral X-ray and UV modelling and analysis software (SPEX, Kaastra et al., 1996) version 3.04.00, which uses an extensive atomic database SPEXACT (version 2.07.00). Apart from the classical Levenberg-Marquardt minimisation of χ^2 algorithm, SPEX allows fitting using the C-statistic (Cash, 1979), defined for Poissonian distribution of data. This is particularly useful for spectra with a low number of counts in a large set of bins where the distribution is far from being Gaussian (and would thus require extensive binning which leads to a decrease in energy resolution) and which is also the case of our data. Use of C-statistic is limited to spectra with a positive number of counts per bin, hence they were binned to at least one count per bin. We employed this statistic for the fitting of projected spectra, using a model constructed in the following form.

As the X-ray emitting gas can be described as a dilute plasma in collisional ionization equilibrium, we used the corresponding model `cie` in SPEX. At the energy resolution of EPIC instruments, the gas spectral properties are set mainly by the temperature of the gas, its amount, which translates to a normalisation of the spectrum, and elemental abundances. As the latter were not possible to constrain properly, we assumed Solar abundances of Lodders et al. (2009) and left free only the overall metallicity of the gas. The fact that the gas temperature is not constant over the volume of the atmosphere was accounted for by parameter `sig`. When non-zero, this parameter changes the model from single- to multi-temperature with a Gaussian distribution and the root-mean-square width equal to `sig`. It is obvious that the assumption of temperature distribution is not necessarily realistic, but still it serves as a good approximation and adds only one free parameter to our model. Other

Table 3.2: Total hydrogen column densities taken from Kalberla et al. (2005).

NGC	1961	3607	3665	4382	4459	4526	4649	5353
$N_{\text{H,tot}} [10^{20} \text{ cm}^{-2}]$	11.7	1.36	2.00	2.54	2.67	1.47	2.04	0.954

commonly used approaches are e.g. two `cie` components with one temperature being tied to the second and by a factor of two smaller, or a different available component with a given temperature distribution, neither of which would be better physically motivated.

Low-mass X-ray binaries (LMXBs) present mainly in globular clusters were modelled with one power-law component with spectral index 1.6, in accordance with Irwin et al. (2003). Absorption by cold Galactic gas (at $z = 0$) was represented by a model `hot` with the temperature set to 5×10^{-4} keV and column density of absorbing medium taken from Leiden/Argentine/Bonn Survey (Kalberla et al., 2005, Table 3.2) and fixed. Similarly, we assume the redshift of the source (Table 2.1) to be known precisely and keep it fixed. The spectra were fitted in the energy range of 0.5 – 5.0 keV, given that the examined X-ray atmospheres produce most of the X-ray emission up to 2.0 keV, while more energetic photons come mainly from a less steep decrease of the power-law component describing the LMXBs. The lower limit on used energy is set by limitations on proper calibration of incoming photons. From this range, events at 1.38 – 1.60 keV were excluded where contamination from instrumental lines (e.g. Carter and Read, 2007) was present.

3.4.1 Deprojection

With the hot gas being optically thin, the observed emission originates in the whole volume of the atmosphere, which inevitably leads to effects related to projection in the observed spectra. Several possibilities for treatment of the data in such a situation exist, all of which are based on the assumption of spherical symmetry of the extended X-ray source.

The method adopted in this work is the so-called Direct X-ray Spectra Deprojection (DSDEPROJ, Russell et al., 2008). As the name suggests, spectra extracted from individual annuli are, after scaling by area, subtracted from those lying closer to their common centre. In order to prevent bins with a negative number of counts, the spectra are binned to at least 25 counts per bin. Unfortunately, spectra created with this method cannot be fitted using C-statistic, so χ^2 minimisation was used instead.

In the following chapters, results are given with 1σ error bars and are derived for a flat cold dark matter cosmology with $H_0 = 70 \text{ km s}^{-1} \text{ Mpc}^{-1}$ and $\Omega_{\text{M}} = 0.3$, $\Omega_{\Lambda} = 0.7$. Hereafter, the gas temperature is presented in units of equivalent energy, $k_{\text{B}}T$.

Results

4.1 Hot gas morphology

As will be discussed in the following section, the hot gas dominates the X-ray emission in the energy range of 0.3 – 2.0 keV. In order to examine morphological features and verify our assumptions on spherical symmetry, we created images from the event files including only the events corresponding to these energies. The final products, i.e. background subtracted, exposure corrected and adaptively smoothed images developed using tasks from Snowden and Kuntz (2011), are presented in Fig. 4.1. The signal is displayed in a logarithmic scale so that the hot atmospheres are visible out to their outskirts while at the same time, bright point sources are removed in the same manner as for the spectral analysis.

To determine the flattening of the atmospheres, we used the CIAO (version 4.11, Fruscione et al., 2006) fitting tool Sherpa (Refsdal et al., 2009) to fit each of them with a 2D β -model (Cavaliere and Fusco-Femiano, 1976, 1978) in a form of

$$I(r) = I_0 [1 + r^2]^{-3\beta/2}, \quad (4.1)$$

where

$$r^2 = \frac{(1 - \varepsilon_X)^2 \tilde{x}^2 + \tilde{y}^2}{r_0^2 (1 - \varepsilon_X)^2} \quad (4.2)$$

and

$$\begin{aligned} \tilde{x} &= (x - x_0) \cos \theta + (y - y_0) \sin \theta, \\ \tilde{y} &= (y - y_0) \cos \theta - (x - x_0) \sin \theta, \end{aligned} \quad (4.3)$$

with normalisation I_0 , the β parameter, the centre of the emission $[\tilde{x}, \tilde{y}]$, orientation determining angle θ , and ellipticity ε_X left free. Parameters of interest, ε_X and position angle $\text{PA}_X = \theta + 90^\circ$ are listed in Table 4.1 along with the ellipticity and position angle of stellar component taken from the literature. It is immediately obvious that the position angles are generally very similar. The measured ellipticity is on average lower in the X-ray component but does not correlate directly with the ellipticity of the stellar component. We note that some of the observed X-ray photons originated in low-mass X-ray binaries and other stellar sources and we are therefore not probing the hot gas alone.

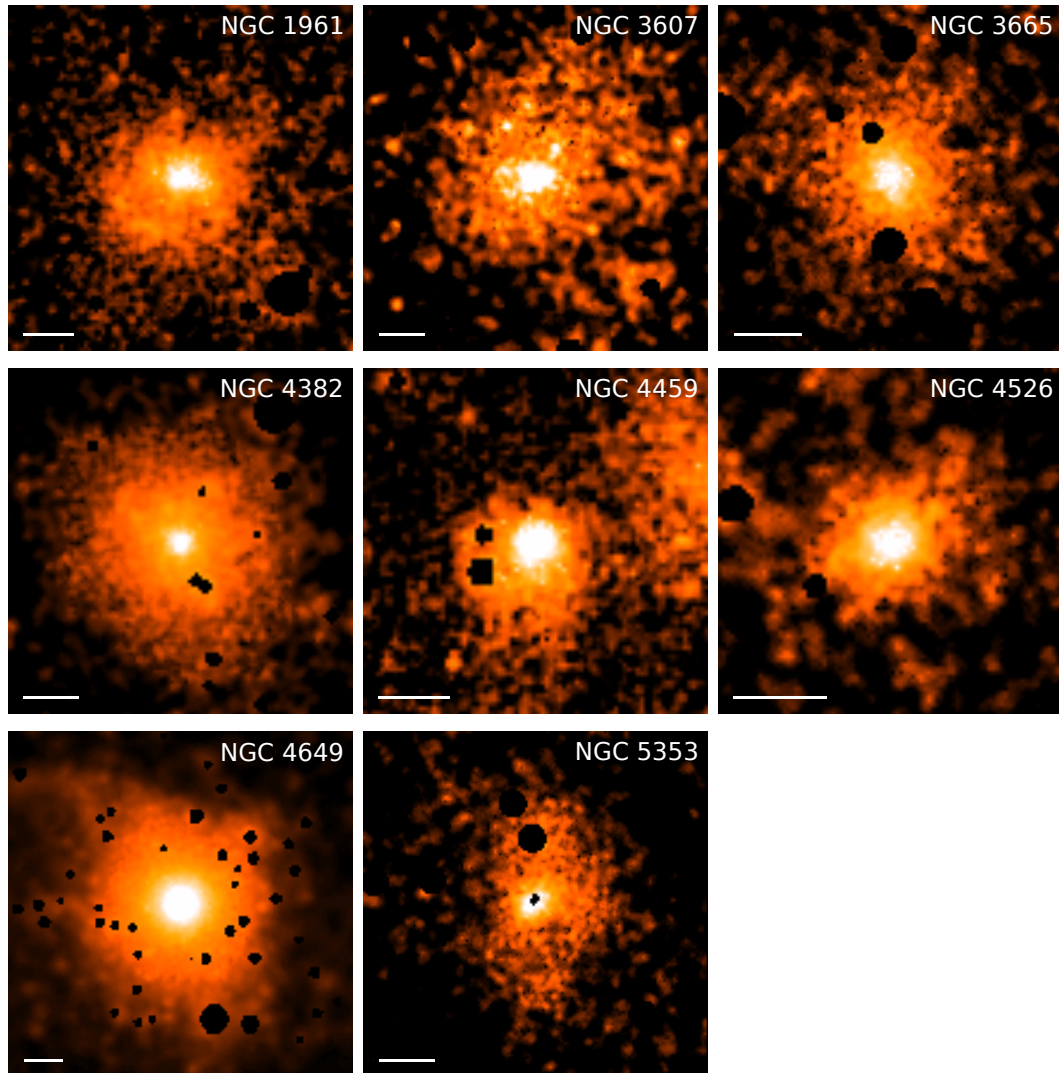


Figure 4.1: Images of X-ray atmospheres of S0 galaxies in our sample, NGC 1961 and NGC 4649, all extracted in the energy range $0.3 - 2.0$ keV. The images are displayed in log-scale in order to visualize the full extent of the hot haloes, while the most prominent point sources are removed. The solid line in the lower-left corner of every image represents a scale of 1 arcmin.

Table 4.1: X-ray ellipticity ε_X and position angle (PA_X) determined from β -model fitting and their optical counterparts, ε_* and PA_* , from Krajnović et al. (2011) and Jarrett et al. (2003) in the case of NGC 1961, for which the uncertainty has not been published.

object	ε_X	ε_*	PA_X [deg]	PA_* [deg]
NGC 3607	0.144 ± 0.011	0.13 ± 0.08	119.7 ± 2.3	124.8 ± 7.6
NGC 3665	0.158 ± 0.005	0.22 ± 0.01	28.2 ± 1.0	30.9 ± 2.0
NGC 4382	0.110 ± 0.006	0.25 ± 0.07	29.8 ± 1.7	12.3 ± 11.0
NGC 4459	0.060 ± 0.016	0.21 ± 0.03	134.1 ± 7.8	105.3 ± 1.9
NGC 4526	0.218 ± 0.005	0.76 ± 0.05	116.8 ± 0.7	113.7 ± 1.2
NGC 5353	0.253 ± 0.004	0.48 ± 0.04	136.6 ± 0.6	140.4 ± 4.9
NGC 1961	0.161 ± 0.009	0.330	100.8 ± 1.8	92.0 ± 2.0
NGC 4649	0.041 ± 0.002	0.16 ± 0.01	90.7 ± 1.6	91.3 ± 3.6

The influence of the surrounding medium on the X-ray emitting gas is clearly visible in several objects. Observable deviation from radial symmetry in NGC 3607 may indicate ram-pressure stripping due to the motion of the galaxy within the intra-group medium. The Leo II group has bi-modal X-ray brightness distribution (with the second X-ray peak centred on NGC 3608 galaxy) and according to Mulchaey et al. (2003) the group members could be in a process of merging.

Ram-pressure stripping is more pronounced in NGC 4459, where an X-ray emitting tail formed and visualises the direction of tangential motion of the galaxy within the Virgo cluster. An X-ray source on the right from NGC 4459 in Fig. 4.1 has been excluded from the spectral analysis. Based on available images from optical telescopes, it cannot be attributed to a nearby galaxy cluster, where individual galaxies should be clearly observable in optical images. We discuss the possible nature of this source in Chapter 5.

In the case of NGC 5353, the position of the centre of the galaxy lies in mutually overlapping chip gaps and bad pixels and therefore there is the black spot in the centre of the X-ray image as no emission could be detected. The point source removed in the upper part of the extended emission can be geometrically attributed to an AGN in NGC 5354 and the surrounding diffuse emission probably forms its hot atmosphere. On the opposite side from this source, another enhancement in surface brightness was detected, but in this case, an optical counterpart cannot explain its presence. As in the previous case, this region has been also excluded from spectral analysis.

As was already mentioned in the previous chapter, NGC 4649 is undergoing ram-pressure stripping and the effects of this process are observable in the outskirts of the detected X-ray emission.

In the rest of this chapter, the results are derived from spectra extracted from concentric annular regions and the error bars on radius represent the width of these annuli.

4.2 Thermodynamic properties

Due to the limited energy resolution of EPIC instruments, low-count spectra of diffuse X-ray emitting plasma from galaxies show strong anti-correlation between gas metallicity and normalisation, as models with enhanced metallicity are statistically indistinguishable from models with lower metallicity but increased normalisation (see Fig. 4.2 for an illustration). The resulting degeneracy can be removed or at least reduced by increasing the number of counts. As no other observations were available, the photon count increase could only be obtained by enlarging the geometric region for the spectrum extraction. This ultimately leads to a combination of photons emitted from the gas of different properties and thus a formation of a multicomponent spectrum of the gas. This, unfortunately, further complicates the situation and does not result in any improvement in metallicity determination.

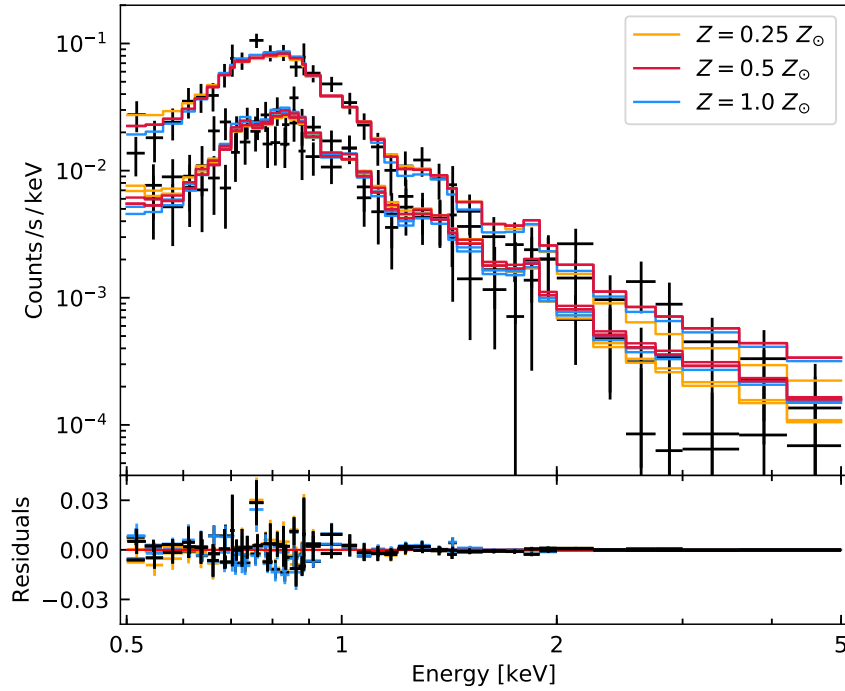


Figure 4.2: Background subtracted spectrum of X-ray emission from the second radial bin of NGC 5353 from all three instruments. Orange, red, and blue lines are best-fitting models composed of redshifted and absorbed *cie* and a power law component, where normalisations for the latter two components are allowed to vary, just as the *cie* temperature. All three provide a good fit to the data. Residuals below the spectrum are black for the metallicity used throughout, $Z = 0.5 Z_{\odot}$, and orange and blue for $0.25 Z_{\odot}$ and $1.0 Z_{\odot}$, respectively. The fit was performed on unbinned data. Due to a larger effective area, the spectrum of pn instrument lies above those of MOS1 and MOS2.

For almost all spectra in our analysis suffer from this degeneracy, we fixed the overall metallicity of the gas to $0.5 Z_{\odot}$, which is a reasonable estimate based on the origin of the gas (stellar mass loss and accretion of intergalactic medium with a low

Table 4.2: Total X-ray gas luminosity, emission-weighted temperature obtained from global spectra, and mass. Where a single temperature model did not provide a good fit, a multi-temperature model was used and the best-fitting value of the additional parameter σ_{T_X} is presented.

object	L_X $10^{40} \text{ erg s}^{-1}$	$k_B T_X$ keV	σ_{T_X} keV	M_X $10^9 M_\odot$
NGC 3607	1.74	$0.411^{+0.025}_{-0.009}$	–	$1.52^{+0.07}_{-0.17}$
NGC 3665	2.30	$0.312^{+0.006}_{-0.006}$	–	$1.09^{+0.07}_{-0.07}$
NGC 4382	7.97	$0.316^{+0.025}_{-0.024}$	$0.012^{+0.017}_{-0.012}$	$5.26^{+0.10}_{-0.10}$
NGC 4459	0.31	$0.390^{+0.041}_{-0.014}$	–	$0.12^{+0.02}_{-0.02}$
NGC 4526	0.71	$0.260^{+0.013}_{-0.019}$	–	$0.15^{+0.03}_{-0.02}$
NGC 5353	4.21	$0.651^{+0.020}_{-0.020}$	$0.225^{+0.042}_{-0.046}$	$0.49^{+0.03}_{-0.03}$
NGC 1961	4.79	$0.298^{+0.030}_{-0.082}$	$0.202^{+0.082}_{-0.053}$	$6.01^{+0.49}_{-0.46}$
NGC 4649	68.26	$0.879^{+0.001}_{-0.001}$	–	$10.75^{+0.65}_{-0.61}$

level of chemical enrichment) and is commonly used in such situations. The only exception is NGC 4649, for which the metallicity was reliably determined from the fit of the global spectrum, $Z = (0.73 \pm 0.04) Z_\odot$, in accordance with results of Mernier et al. (2017). For the deprojection analysis, the metallicity of this object was set to $0.7 Z_\odot$ and fixed.

4.2.1 Global properties

We estimated the total gas mass M_X of the hot atmosphere by summing total particle number density n derived from deprojected spectra in a given spherical shell, i.e.

$$M_X = 4\pi \sum r^2 \rho(r) \Delta r = 4\pi m_H \mu \sum r^2 n(r) \Delta r, \quad (4.4)$$

where μ is mean atomic weight, $\mu = 0.62$, and m_H is the mass of a hydrogen atom. The particle number density was calculated as $n = 1.92 n_e$, where the electron number density n_e was obtained directly from the spectrum normalisation. The summation has been performed out to the last annulus presented in this work, corresponding to approximately $2 - 6 R_e$, set by the data quality.

The calculated masses are given in Table 4.2. For the density profiles, see Fig. A.2 in the Appendix. We fitted the entire galaxy X-ray gas emission with a single- or multi-temperature model, depending on the spectrum (see sec. 3.4), to obtain global properties of the hot gas. Best-fitting parameters derived from this fit are listed in Table 4.2. Gaussian width of the temperature distribution of multi-temperature model is denoted as σ_{T_X} and is presented for spectra where this model provided a better fit.

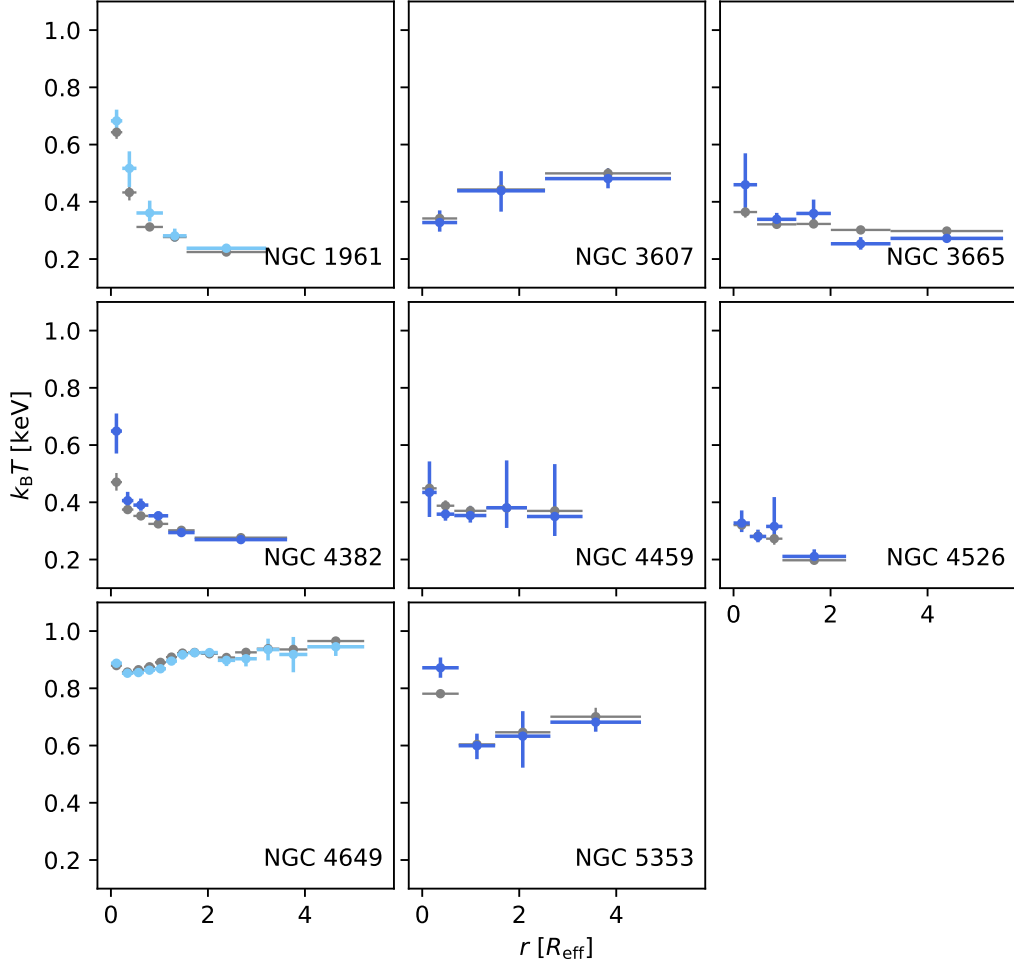


Figure 4.3: Radial, azimuthally averaged profiles of deprojected temperature with metallicity fixed at $0.5 Z_{\odot}$ except for NGC 4649 for which the metallicity is $0.7 Z_{\odot}$. For clarity, dark blue points represent S0 galaxies in our sample, while the spiral galaxy NGC 1961 and the elliptical NGC 4649 are plotted in light blue.

4.2.2 Temperature

The best-fitting temperature obtained directly from both projected and deprojected spectra of every annulus is presented in Fig. 4.3 as a function of effective radius, and thus scaled by the radial extent of the stellar component. Temperature profiles in physical units derived only from deprojected spectra, which we used for the analysis further on, can be found in the Appendix, Fig. A.1. The spiral and elliptical galaxy are plotted in a lighter shade of blue to be easily distinguishable from lenticulars. The most striking feature of the mosaic is that the mean temperature of S0 galaxies is smaller than that of the only elliptical (and more massive) galaxy NGC 4649. Overall, the profiles of S0 galaxies do not show any significant trends and within 3σ uncertainties are close to being isothermal.

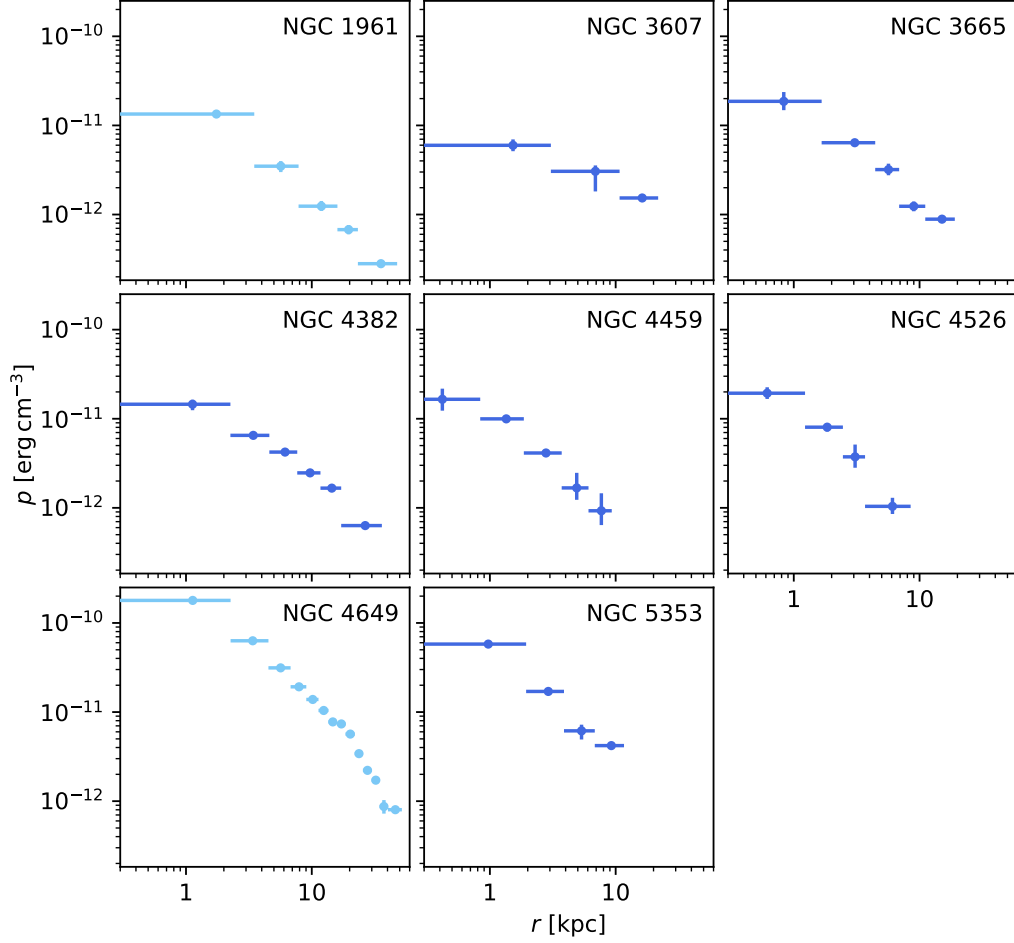


Figure 4.4: Pressure profiles derived from deprojected spectra. Point colour is chosen as in Fig. 4.3 and is kept in remaining figures of this kind further on.

4.2.3 Pressure

The gas pressure as a function of the radius was calculated assuming ideal gas, i.e.

$$p = nk_{\text{B}}T. \quad (4.5)$$

These profiles are shown separately in Fig. 4.4, using the same colour-coding as for the temperature above. In all objects, the pressure is monotonically radially decreasing, which is expected for gravitationally stratified atmospheres. The main difference in profiles of rotating galaxies in our sample (S0s and NGC 1961) and the massive elliptical is the vertical shift within the plot, or in other words, the pressure is almost an order of magnitude higher in NGC 4649 with respect to the remaining seven objects.

When compared to a larger number of elliptical galaxies, namely 49 ellipticals (including NGC 4649) studied by Lakhchaura et al. (2018), the division remains clearly visible, as can be seen in Fig. 4.5. Their profiles are distinguished by a presence and

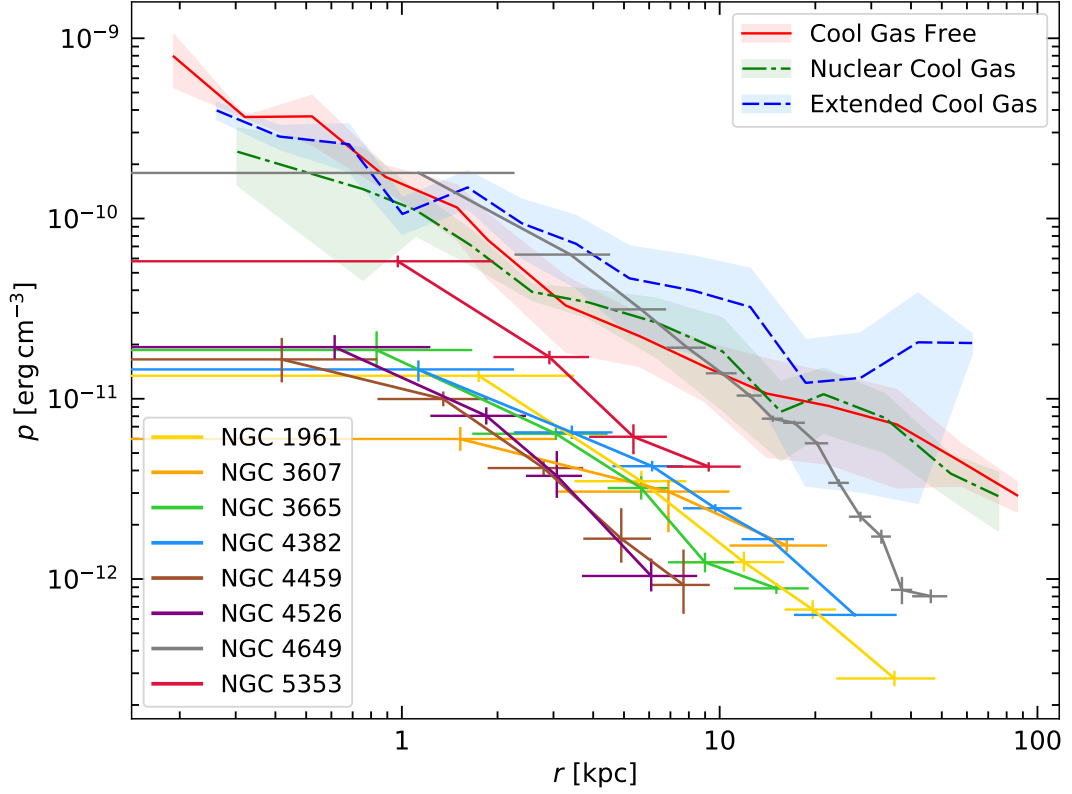


Figure 4.5: Pressure profiles of all eight galaxies (lines) and median profiles of ellipticals (Lakhchaura et al., 2018) distinguished by cool gas content. The shaded regions represent a median absolute deviation spread.

morphology of ‘cool’ (relative to X-ray) gas, more specifically of $H\alpha + [N II]$ emission. The solid red, dot-dashed green, and dashed blue lines stand for median entropy profiles of galaxies undetected in $H\alpha + [N II]$, with nuclear emission and having cool gas with filamentary structure, respectively. The surrounding shaded regions represent median absolute deviation (MAD). Regardless of the cool gas content in their sample (further discussed in the text below), the pressure in S0s is lower at all radii. One of the reasons for this difference lies in the total mass of these galaxies. Ellipticals are known to be generally more massive than lenticular galaxies and the difference in gravitational potential should also reflect in the gas pressure. Rotation can further lower the effective potential, allowing the gas to remain more dilute.

To limit the effect of different total mass, the radial distances need to be plotted in properly scaled units. The determination of the total enclosed mass $M(\leq r)$ within some radius r is computable from the thermodynamic properties of the gas, i.e.

$$\frac{dp}{dr} = -\frac{GM(\leq r)\rho}{r^2}, \quad (4.6)$$

assuming spherically symmetric atmosphere in hydrostatic equilibrium and a negligible effect of non-thermal pressure. This, after a reorganisation and a substitution for the

gas density, $\rho = m_{\text{H}}\mu n$, yields

$$M(\leq r) = -\frac{r^2}{Gm_{\text{H}}\mu n} \frac{dp}{dr}. \quad (4.7)$$

Mass-scaled radius is then usually defined through the mean enclosed density in units of the critical density of the Universe,

$$\rho_c = \frac{3H_0^2}{8\pi G}, \quad (4.8)$$

where we assume the Hubble constant $H_0 = 70 \text{ km s}^{-1} \text{ Mpc}^{-1}$. The scale radius r_{Δ} , representing the distance from the galaxy centre at which the mean enclosed density is equal to $\Delta\rho_c$, is given simply through

$$\rho_{\Delta} = \Delta\rho_c = \frac{M(\leq r_{\Delta})}{\frac{4}{3}\pi r_{\Delta}^3}. \quad (4.9)$$

After substitution with (4.7) and several simplifications, it can be written as

$$\frac{\Delta}{2}H_0^2 = -\frac{1}{m_{\text{H}}\mu} \frac{1}{r_{\Delta}n(r_{\Delta})} \frac{dp}{dr} \Big|_{r_{\Delta}}. \quad (4.10)$$

For a direct comparison with the scale radius obtained differently, we set $\Delta = 200$. Solving numerically this equation, we obtained values of r_{200} listed in Table 4.3. For the pressure gradient, we use a functional form in the calculation. The pressure can be well described by β -profile (Cavaliere and Fusco-Femiano, 1976, 1978), defined as

$$p(r) = p_0 \left[1 + \left(\frac{r}{r_c} \right)^2 \right]^{-3\beta/2}, \quad (4.11)$$

where the core radius r_c , central pressure p_0 and parameter β are determined from the fit. In the case of NGC 3607, where gas properties have been determined for only three radial distances, a power-law function was assumed instead. Particle density n is also expressed as a function of radius, assuming a β -profile or a power law again.

However, the requirement of hydrostatic equilibrium is obviously not fulfilled in rotating systems, and therefore the obtained values should serve only as a rough estimate. The M_{200} for five galaxies in our sample, among others, has been determined by James et al. (2018). In that work, an independent method has been used, employing the kinematics of globular clusters to determine the total mass of the galaxy, or using the total stellar mass of globular clusters as a proxy for the total gas of the galaxy, as the two have been found to correlate. The values of $r_{200, \text{GC}}$ derived from these measurements are listed also in Table 4.3. For NGC 1961 we adopt r_{200} determined in Bogdán et al. (2013) from baryonic Tully-Fisher relation for the cold dark matter cosmogony, $M_{200} \propto V_{\text{max}}^{3.23}$, where V_{max} is the maximum rotational velocity of the galaxy. Even though likely more accurate than the one derived from X-ray gas properties, this value should be regarded also as an estimate. Plotting the pressure profiles of S0s against r_{200} along with ellipticals (Fig. 4.6), the dichotomy is still clearly visible. The

Table 4.3: Scale radius $r_{200, X}$, derived from X-ray observations, and $r_{200, GC}$, which has been determined from globular clusters kinematics or the total mass of galaxy’s globular clusters from James et al. (2018). *The value has been determined from maximal stellar rotation velocity in Bogdán et al. (2013).

NGC	1961	3607	3665	4382	4459	4526	4649	5353
$r_{200, X}$ [kpc]	213.1	410.4	272.0	295.7	677.7	236.7	730.0	829.5
$r_{200, GC}$ [kpc]	470*	396.1		491.0	345.0	402.2	749.0	

dashed grey line represents a median profile of pressure in 19 ellipticals of Lakhchaura et al. (2018), for which the $r_{200, GC}$ is also known from the globular clusters properties, and the grey-shaded region shows the corresponding median absolute deviation. S0s are further distinguished by a rotational velocity, showing no observable systemic trend.

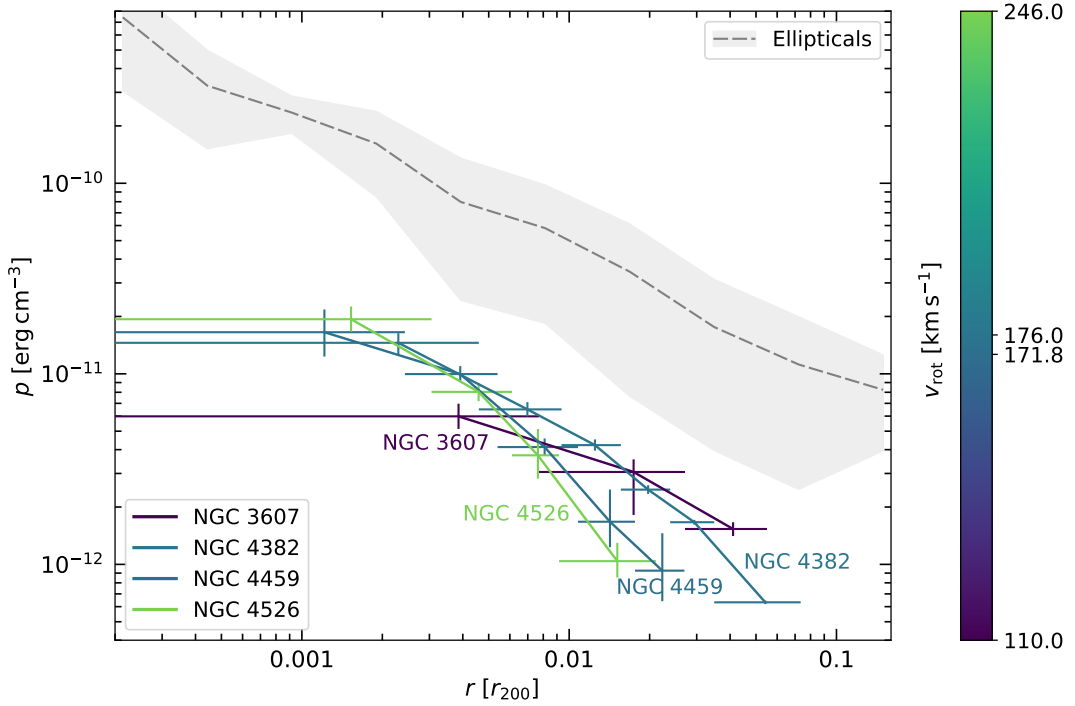


Figure 4.6: Deprojected pressure profiles of S0s with known $r_{200, GC}$, displayed in the scale radius which was obtained by a method independent of dynamical properties of the galaxies. The dashed grey line stands for a median profile of elliptical galaxies studied in Lakhchaura et al. (2018) and the surrounding grey region defines the median absolute deviation spread. The rotational velocity of the galaxy is represented by the line colour.

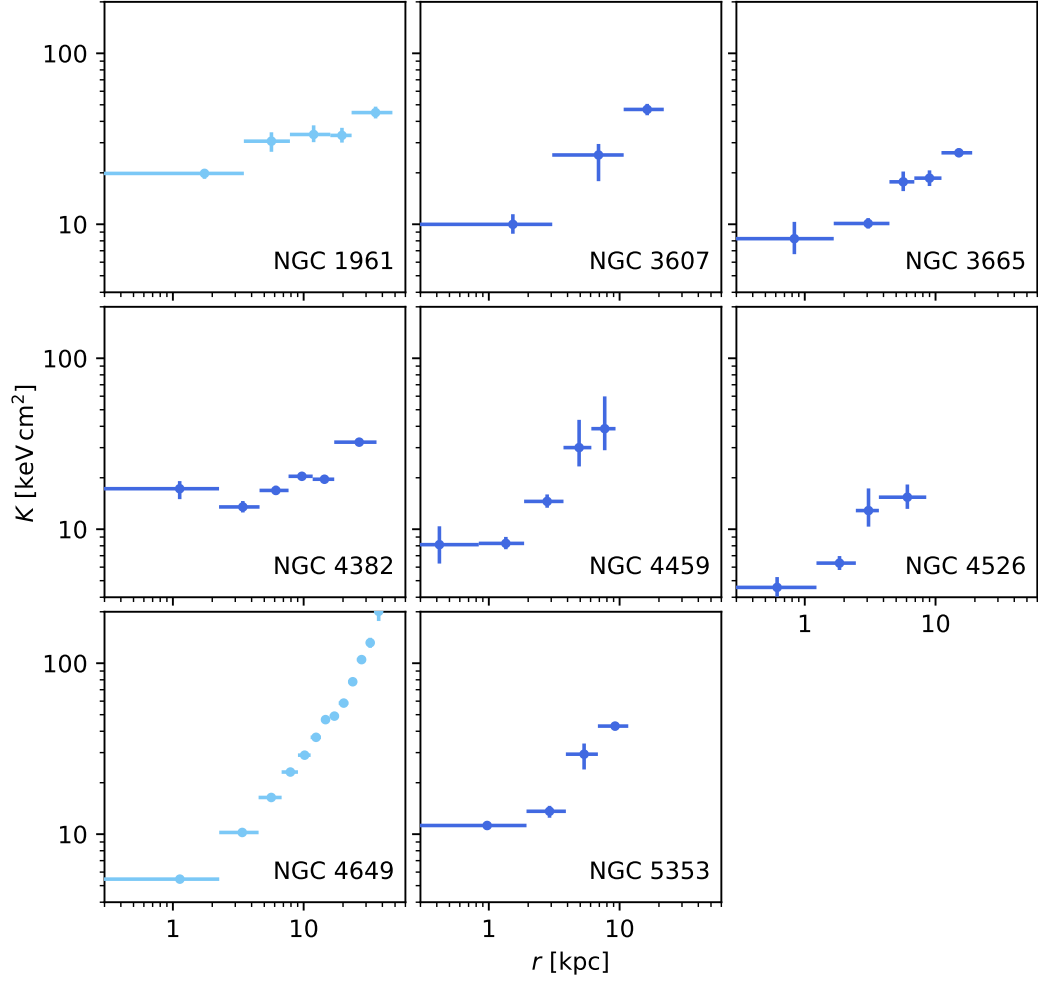


Figure 4.7: Entropy profiles (see equation 4.12) derived from deprojected spectra.

4.2.4 Entropy

Another physical quantity which describes the thermodynamic state of a hot atmosphere is entropy. Its broadly adopted definition in this context comes from the equation describing the adiabatic process in a monoatomic ideal gas, $pV^{5/3} = \text{const}$. Rewriting this relation in terms of temperature and electron density, the constant is proportional to K , our measure of entropy, where

$$K \equiv k_B T n_e^{-2/3}. \quad (4.12)$$

This definition relates to the thermodynamic entropy S as $\Delta S = 3/2 \ln K$. Gravitationally stratified atmosphere in hydrostatic equilibrium should have the radial entropy profile monotonically outwardly rising, while flat or decreasing trend signifies convectively unstable environment. This results from the Schwarzschild stability criterion,

$\nabla K \cdot \nabla p < 0$, where the gas pressure p is radially decreasing due to gravitational stratification (see the previous section). A detailed derivation of this condition can be found in e.g. Pringle and King (2007).

The entropy of all analysed galaxies is separately plotted in Fig. 4.7 and shows a visible difference in the slope of NGC 4649 when compared to our S0s. For a more robust comparison with elliptical galaxies, the entropy profiles of S0s are plotted in Fig. 4.8, together with results obtained for the sample of 49 elliptical galaxies presented by Lakhchaura et al. (2018) again. The extent of H α emitting gas has been searched for and observed only in two galaxies in our sample, NGC 4459 and NGC 4526. A direct comparison for the remaining four objects is thus possible only with the (reasonable) assumption that the colder phases are accompanied by ionized gas with similar morphology. Another system with observed H α and rotating [C II] discs, and thus having the presumed properties, a lenticular galaxy NGC 7049, is bridging together with NGC 4459 and NGC 4526 the two samples. Its profile, instead of following the extended cool gas region of ellipticals, lies above it, similarly to our S0s. Furthermore, the mean central entropy of the lenticulars lies above that observed in elliptical galaxies.

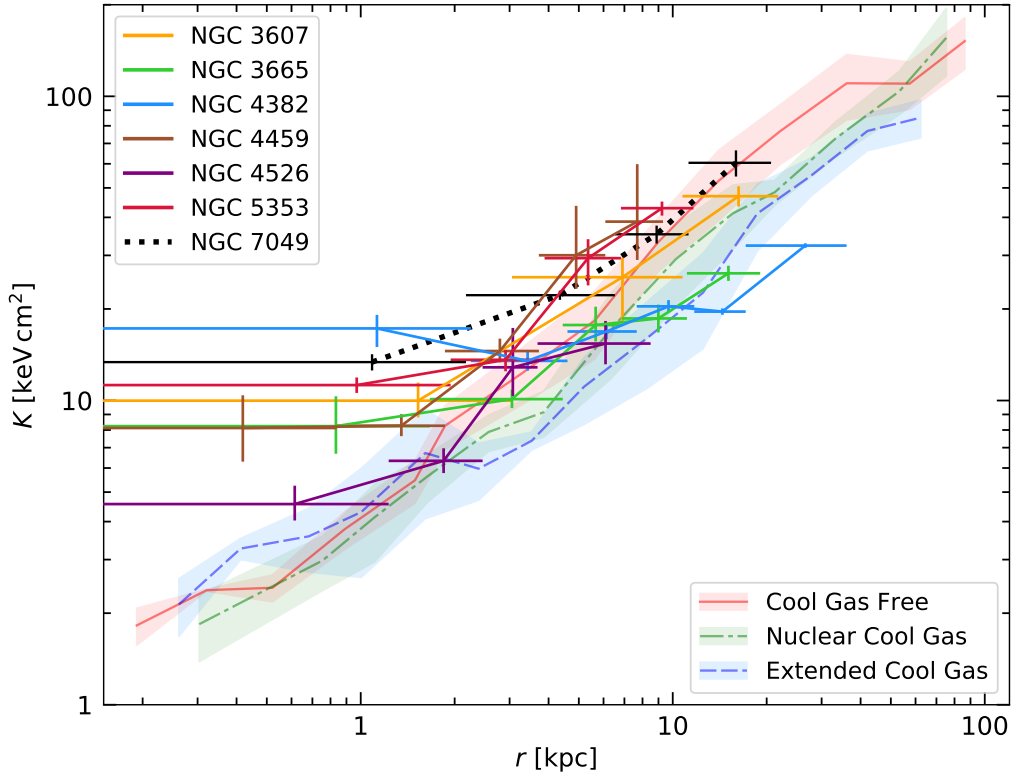


Figure 4.8: Entropy profiles of S0 galaxies in this study (solid lines), NGC 7049, an S0 from previous work (Juráňová et al., 2019, black dotted line) and a sample elliptical galaxies distinguished by the extent of cool gas of Lakhchaura et al. (2018). For the ellipticals, lines signify median profiles and surrounding shaded regions the median absolute deviations.

Purely gravitational heating would result in a profile given by $K \propto r^{1.1}$, which is usually not observed due to the contribution of AGN-related heating and SNe. These processes centrally increase the gas entropy, flattening the whole profile in isolated galaxies or central regions of galaxy clusters to $K \propto r^{0.67}$ (Panagoulia et al., 2014; Babyk et al., 2018b). To quantify the amount of flattening in rotating atmospheres, we fitted the entropy profiles of all S0 galaxies in our sample with a power-law model, together with a fast-rotator NGC 1961 and including also S0 galaxies NGC 4477 (Li et al., 2018) and NGC 7049 (Juráňová et al., 2019), and an E2 galaxy NGC 6868 (Werner et al., 2014; Lakhchaura et al., 2018), all having rotating discs of warm/cold gas indicative of rotational support. The resulting profile yields a power-law index $\Gamma = 0.46 \pm 0.05$ and the corresponding best fitting curve is plotted together with all used data in Fig. 4.9.

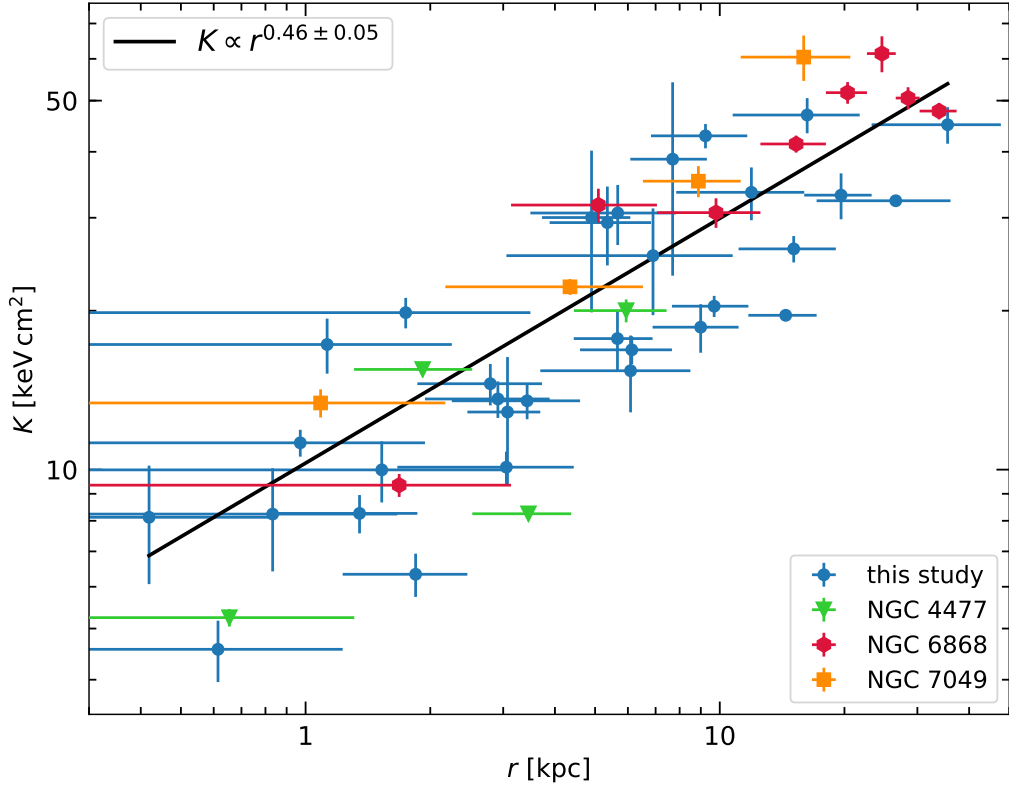


Figure 4.9: Entropy profiles of rotationally supported galaxies in this study together with profiles of NGC 4477 (Li et al., 2018), NGC 7049 (Juráňová et al., 2019), and NGC 6868 (Werner et al., 2014; Lakhchaura et al., 2018). The black line represents a best-fitting power law model determined from a fit of all plotted data points.

4.3 Thermal stability

Higher central entropy suggests recent heating of the atmospheres. AGN activity has been confirmed in NGC 3665 (see section 2.3) and *Chandra* observations show an X-ray point source emission in the centre of NGC 3607, NGC 3665, NGC 4459, and NGC 4526. Therefore, to address the thermal stability of the gas, we computed cooling time profiles using the definition (1.1), which are shown in Fig. A.4 in the Appendix.

In addition to cooling time alone, profiles of cooling time to free-fall time ratio were derived from the observed thermodynamic properties. The free-fall time (1.2) was computed using gravitational acceleration

$$g = -\frac{1}{\rho} \frac{dp}{dr} = -\frac{1}{nm_{\text{H}}\mu} \frac{dp}{dr}, \quad (4.13)$$

and thus under the assumption of hydrostatic equilibrium. The resulting values are presented in Fig. 4.10 for all eight studied objects and separately in the Appendix, Fig. A.3. The $t_{\text{cool}}/t_{\text{ff}} \approx 10$ boundary is visualised through the dashed grey line and is exceeded at all radii, in consistency with observations of other early-type galaxies and galaxy clusters (Voit et al., 2018). We note that the $t_{\text{cool}}/t_{\text{ff}}$ ratio is fundamentally independent of radius and thus no common trend is expected nor observable in Fig. 4.10.

Computation of the C -ratio (1.3) requires knowledge of the velocity dispersion $\sigma_{v,L}$ at the distance where the turbulence is injected, or the injection scale length, L . According to Gaspari et al. (2018), this distance can be estimated as a diameter of

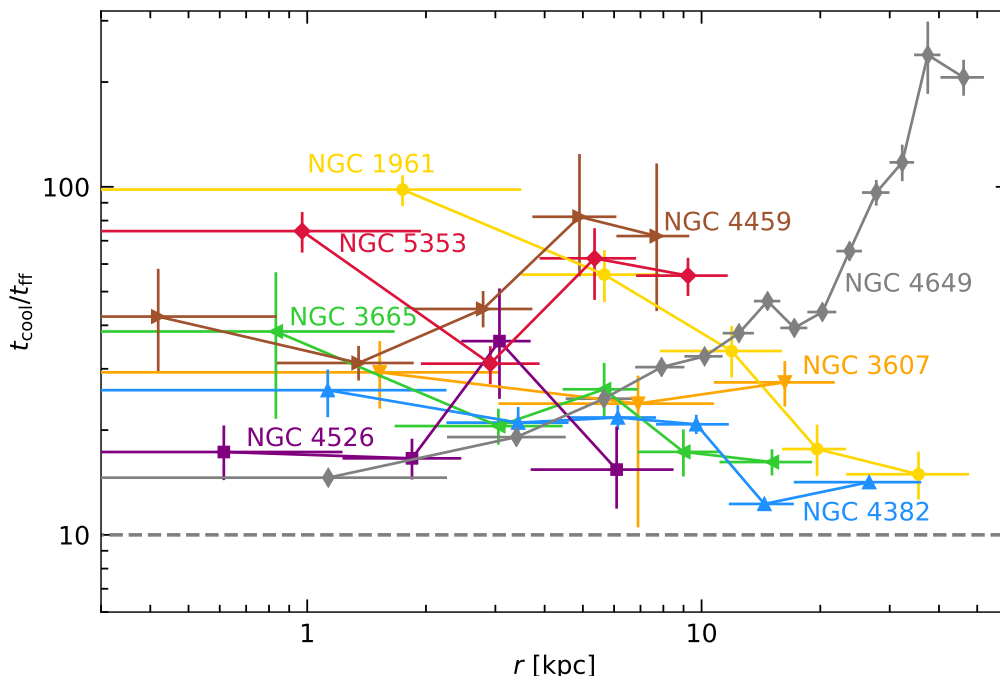


Figure 4.10: Ratio of cooling time and free-fall time of all studied galaxies. The threshold of $t_{\text{cool}}/t_{\text{ff}} \approx 10$ (see section 1.3) is visualised as a dashed grey line.

the cold/warm phase, and the corresponding $\sigma_{v,L}$ can be obtained by extrapolating from measured σ_v of the cold gas. For galaxies in our sample, these measurements have not been published to date. Nevertheless, to have at least an estimate of this condensation parameter, we adopt the value of velocity dispersion measured in NGC 7049, $\sigma_{v,L} = 36 \text{ km s}^{-1}$, and use it for our calculations. The results computed for S0 galaxies with discs of cold gas are plotted in Fig. 4.11 and show that conditions in these hot haloes are in favour of condensation from the hot phase.

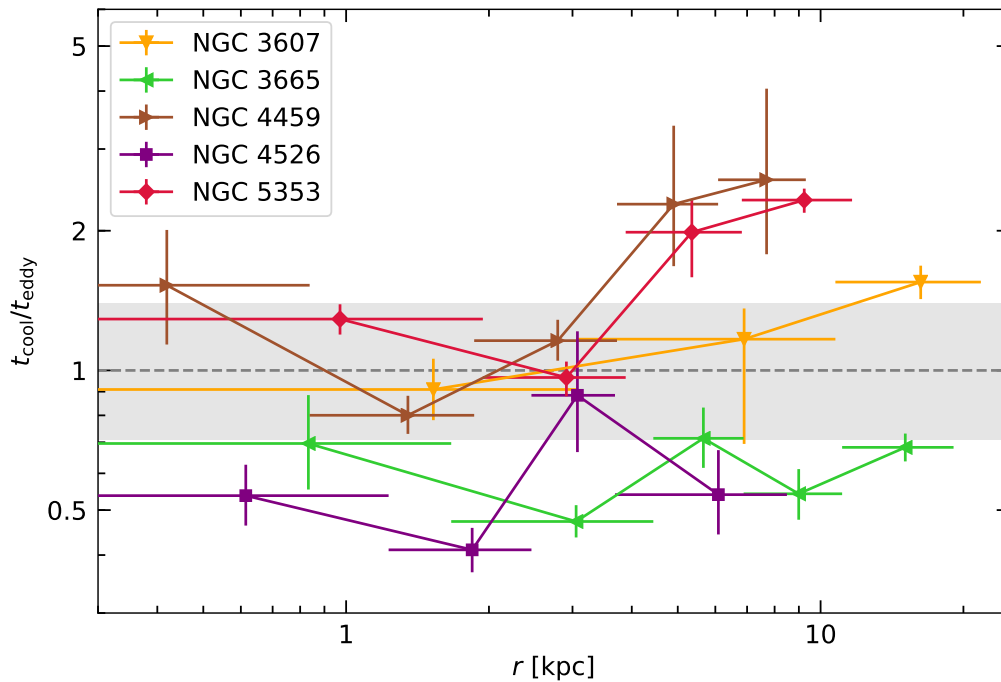


Figure 4.11: C -ratio (see equation 1.3) of S0 galaxies possessing cold gas. Grey region represents the 1σ confidence region (from hydrodynamical simulations; Gaspari et al., 2018) signifying conditions for development of multiphase condensation.

Discussion

5.1 Hot gas morphology and mass

Projected flattening of the hot atmospheres has been found to be similar to or smaller than that of stellar component in all studied objects, in accord with hydrodynamical simulations of Negri et al. (2014). It needs to be emphasized that the ellipticity has been measured on X-ray images (background and point sources subtracted), with contamination of remaining X-ray emission from unresolved LMXBs, which could further amplify the observed flattening. However, given that the X-ray emission at 0.3 – 2.0 keV is dominated by the hot gas, the ellipticity is primarily given by the diffuse gas. Remarkably, the principal axes of the ellipsoidal isophotes fitted to X-ray and optical emission are aligned within the measured uncertainties. This finding, together with the non-zero ellipticity, is consistent with ordered rotation of the X-ray atmospheres in a generally rounder total gravitational potential.

The assumption of spherical symmetry is therefore not formally accurate. However, the intrinsic scatter given by the quality of data limited by the number of obtained counts and also the spatial resolution of *XMM-Newton* reduces the effects of this simplification. Furthermore, it is important to keep in mind that the ellipticity of the X-ray atmospheres is low and that the logarithmic scale in Fig. 4.1 emphasizes features beyond azimuthal symmetry. Overall, the assumption of spherical symmetry is not expected to affect our results significantly.

The amount of observed hot gas in S0 galaxies, which has been derived from deprojected densities out to $2 - 6 R_e$, varies from 10^8 to $5 \times 10^9 M_\odot$. The largest amount has been found in NGC 4382 and is comparable to hot gas content in NGC 1961, while the hot gas mass of the massive slow-rotating elliptical is about two times larger. Negri et al. (2014) showed that rotationally supported galaxies of the same mass have, besides lower X-ray luminosity and emission-weighted temperatures, also a lower amount of hot gas. Here, a comparison based on the same approach is not possible, as within this small sample the galaxies vary both in rotation and the total galaxy mass and could have also been affected by the surrounding environment.

5.1.1 Diffuse emission near NGC 4459

A source of diffuse X-ray emission near the hot atmosphere of NGC 4459 is shown in the left panel of Fig. 5.1. The projected direction of motion of NGC 4459 within the Virgo

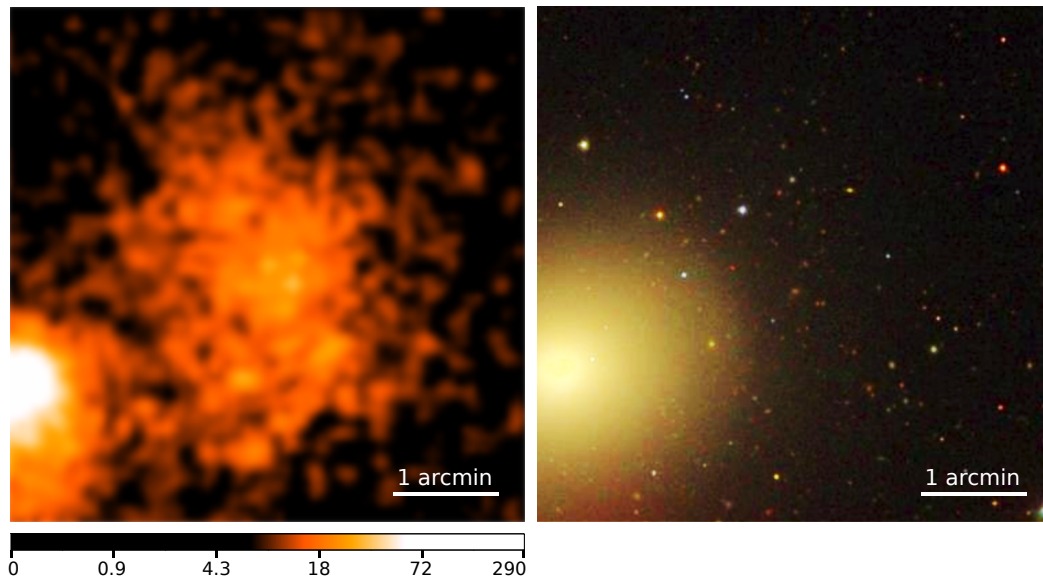


Figure 5.1: Left: Background subtracted, exposure corrected and adaptively smoothed X-ray image centred on diffuse emission near NGC 4459 and extracted from energy range $0.3 - 2.0$ keV, at which most of the emission can be observed. The colour bar, showing the number of received counts, allows a qualitative comparison of flux from NGC 4459 and the diffuse source. Right: geometrically corresponding region of the sky observed in SDSS (data release 9). No nearby counterpart is observable, but the faint red galaxies could signify a distant cluster.

cluster, as traced by ram-pressure stripped gas (see Fig. 4.1), and the direction from the galaxy to the diffuse source form an angle of $\sim 65^\circ$. This extended emission shows an enhancement in brightness towards its centre (at approximately $\alpha = 12^{\text{h}} 28^{\text{m}} 51^{\text{s}}$, $\delta = +13^\circ 59' 36''$). The total number of observed net counts from all instruments and both observations is 8972 with an energy flux $f \approx 2.5 \times 10^{-9} \text{ erg s}^{-1} \text{ m}^{-2}$. However, no lines are visible in the spectrum, which complicates a determination of the redshift. No counterpart has been observed in UV (*Galex*), near-infrared (2MASS observations in *J*, *H*, *K* bands), mid-infrared (*Spitzer*), far-infrared (*Herschel* PACS at $70 \mu\text{m}$ and $160 \mu\text{m}$), or sub-millimetre wavelengths (*Herschel* SPIRE at $250 \mu\text{m}$, $350 \mu\text{m}$, and $500 \mu\text{m}$).

In the right panel of Fig. 5.1, an optical image from SDSS covering the same area as the X-ray image reveals a number of distant red galaxies. To test whether the X-ray emission could belong to a galaxy cluster with galaxies observable by SDSS, we calculated luminosity for a maximum redshift at which galaxies have been detected, $z \sim 0.7$ (Brescia et al., 2014). The resulting X-ray luminosity $L_X \approx 1 \times 10^{44} \text{ erg s}^{-1}$ is common among galaxy clusters (see e.g. Pratt et al., 2009).¹

¹Shortly before handing in the thesis, we found out that this source has been classified in the XCLASS catalogue as a galaxy cluster based on follow-up observations in optical and infrared bands and has photometrically determined redshift of $z = 0.5$ (Ridl et al., 2017). This object has been assigned a catalogue number 2260 and is listed in an internal database.

5.2 Thermodynamic properties

The thermodynamic properties derived from the X-ray spectra are dependent on the validity of our assumption on the chemical composition of the plasma. In fact, the projected spectra available for our analysis allowed us to constrain the metallicity in several cases, and we present the obtained best-fitting values in Fig. A.5. Where measured, some of the profiles show significant variations as a function of radius. In principle, these features can indeed be present in hot atmospheres. A decrease in abundances of heavy elements towards the outskirts of these atmospheres would be caused by a presence of gas previously unenriched in stellar evolution, supplied from the intergalactic medium. At the same time, a central decrease of the overall metallicity could be explained by deposition of heavy elements (excluding noble gases) into dust grains, as has been recently observationally confirmed by Lakhchaura et al. (2019).

A reliable metallicity determination is, however, problematic. Analysing *Chandra* observations, Babyk et al. (2018a) measured the overall metallicity of a hot atmosphere in NGC 5353 to be $Z = (0.17 \pm 0.03) Z_{\odot}$, three times lower than in each radial bin presented in this work. Albeit unusually low (e.g. Mernier et al., 2017), their result is in accordance with findings of Finoguenov et al. (2007) who studied the hot medium of the whole HCG 68 group. We remind, however, that this outcome is expectable for an analysis of multi-temperature spectra fitted with a single-temperature model, as has been thoroughly discussed by Buote (2000).

The conservative approach adopted here, i.e. leaving the metallicity fixed and constant for all radial bins, is therefore usually performed in the spectral analysis. We note that a bias in the overall metallicity would affect the derived physical quantities as follows. A factor of two difference in the measured and actual metallicity would result in 25% bias in the density and pressure, and 17% in the gas entropy. Slopes of radial profiles would be altered by less than 10% in a presence of metallicity gradients (Werner et al., 2012).

As the only spiral galaxy in our sample is currently star-forming, unresolved high-mass X-ray binaries and, to a lesser extent, other stellar sources associated with young stellar populations are also expected to pollute the observed X-ray emission. Similarly to LMXBs, the composite spectrum of these stellar sources also forms a power law, but likely with a different index. However, the results of our analysis are remarkably similar to those presented by Anderson et al. (2016), who also studied the hot atmosphere of NGC 1961 but allowed the power-law index to vary during the fitting procedure to account for all stellar X-ray sources. Therefore, we do not expect our simplification to have a significant effect on the derived physical quantities.

5.2.1 Temperature

Radial azimuthally averaged profiles reveal that the hot gas temperature is systemically lower in the S0 galaxies than in the massive elliptical NGC 4649. This is an expected outcome, as the virial temperature of less massive S0 galaxies is lower and the ordered stellar motion in rotating systems leads to less effective heating (in terms of the

resulting temperature) of the gas ejected in stellar mass loss. Outwardly decreasing temperature in NGC 1961 suggests central heating, which can be provided by an AGN or a higher SN rate, connected to relatively high star formation of $\sim 10 M_{\odot} \text{ yr}^{-1}$.

A negative temperature gradient is observable also in NGC 4382. Provided that this object does indeed not harbour an AGN (see section 2.4), the source of heating should also be connected to the stellar population, possibly enhanced by a merger event. The energy input via type Ia SNe can be estimated from their expected rate, which for a galaxy of this stellar mass ($M_{\star} = 4 \times 10^{11} M_{\odot}$; Gallo et al., 2010) and SFR (see Table 2.2) corresponds to approximately 0.02 yr^{-1} using a relation from Sullivan et al. (2006), or 0.01 yr^{-1} , when derived from the B -band luminosity (Pellegrini, 2012). With kinetic energy of one explosion, $E_{\text{SNIa}} \approx 10^{51} \text{ erg}$ (e.g. Rosswog and Brüggen, 2007), this rate corresponds to a time-averaged energy injection of $6 \times 10^{41} \text{ erg s}^{-1}$ or $3 \times 10^{41} \text{ erg s}^{-1}$, respectively. Such heating would be sufficient to compensate for the energy losses of the hot gas if the efficiency of SN heating was at least $\sim 12\%$ or $\sim 27\%$, respectively. An additional contribution of the merger event that led to the creation of shells is expected to be of lesser importance. According to cosmological numerical simulations analysed by Pop et al. (2018), the initial interaction with the progenitor occurred 4 – 8 Gyr ago and most of the stars were stripped from it ~ 2 Gyr ago, while the central cooling time measured in NGC 4382 is $t_{\text{cool}} \approx 0.5 \text{ Gyr}$.

A higher overall temperature of NGC 5353 could be attributed to the fact that this galaxy is the brightest member of a compact group and to other processes within it (Sun, 2012).

5.2.2 Pressure

Fig. 4.6 shows that the systemically lower pressure cannot be explained solely by different total galaxy masses. Even after scaling by r_{200} , the order of magnitude gap between profiles of lenticulars and ellipticals is still present at all radii. In Fig. 5.2, other general properties are visualised for all studied galaxies: $B - V$ colour index (Table 2.2), the ratio of stellar rotational velocity and velocity dispersion (Table 2.1) and X-ray luminosity and gas mass (Table 4.2). $B - V$ colouring reveals that the pressure is independent of redness of these galaxies, and thus the composition of stellar populations cannot explain the additional pressure support. Using different colour indexes, we obtained qualitatively similar results. At the same time, the absence of any residual dependence on the rotational velocity (Fig. 4.6) and the ratio of rotational velocity and velocity dispersion (Fig. 5.2) suggests that this shift cannot be attributed to rotational support alone.

For ETGs, Pellegrini (2012) claimed that objects with $L_{\text{B}} \lesssim 3 \times 10^{10} L_{\text{B},\odot}$ should be prone to have atmospheres in an outflowing state (see section 1.5). This applies to all S0 galaxies in our sample, perhaps except for a more luminous NGC 4382. The lowered pressure would then be a direct manifestation of an expanding atmosphere. Similarly, this would reflect on the trend in X-ray luminosity and hot halo mass, presented in the bottom panels of Fig. 5.2, but it is necessary to keep in mind that other environmental effects can play a significant role in affecting the hot gas content. It is also important to note that we plot the halo mass measured within a radius determined by the data

quality, which thus does not directly follow the physical properties of the galaxies. However, using values obtained from integration out to e.g. $5R_e$ of extrapolated densities, the trend remains visible and is not significantly altered.

The computed values for $r_{200,X}$ require some commentary as well. The $r_{200,X}$ in NGC 4459 is larger than $r_{200,GC}$, while the rotational support or turbulence, which act against gravity, should result in the opposite outcome. Additionally, other non-thermal pressure sources, such as magnetic fields or cosmic rays can lead to lower values of $r_{200,X}$, if present (see eg. Humphrey et al., 2013). A combination of additional pressure support reflects in results of other S0 galaxies in our sample. A plausible explanation for the large $r_{200,X}$ in NGC 4459 lies in interactions with the surrounding environment. The apparent increase in galaxy total mass results from a steeper decrease of pressure and, at the same time, lower density. Flying through the Virgo cluster, NGC 4459 undergoes ram-pressure stripping and the more loosely bound gas is being removed from the atmosphere. This interaction can lead to both mentioned effects. Similarly, the computed $r_{200,X}$ of NGC 5353 is likely affected by the intragroup environment.

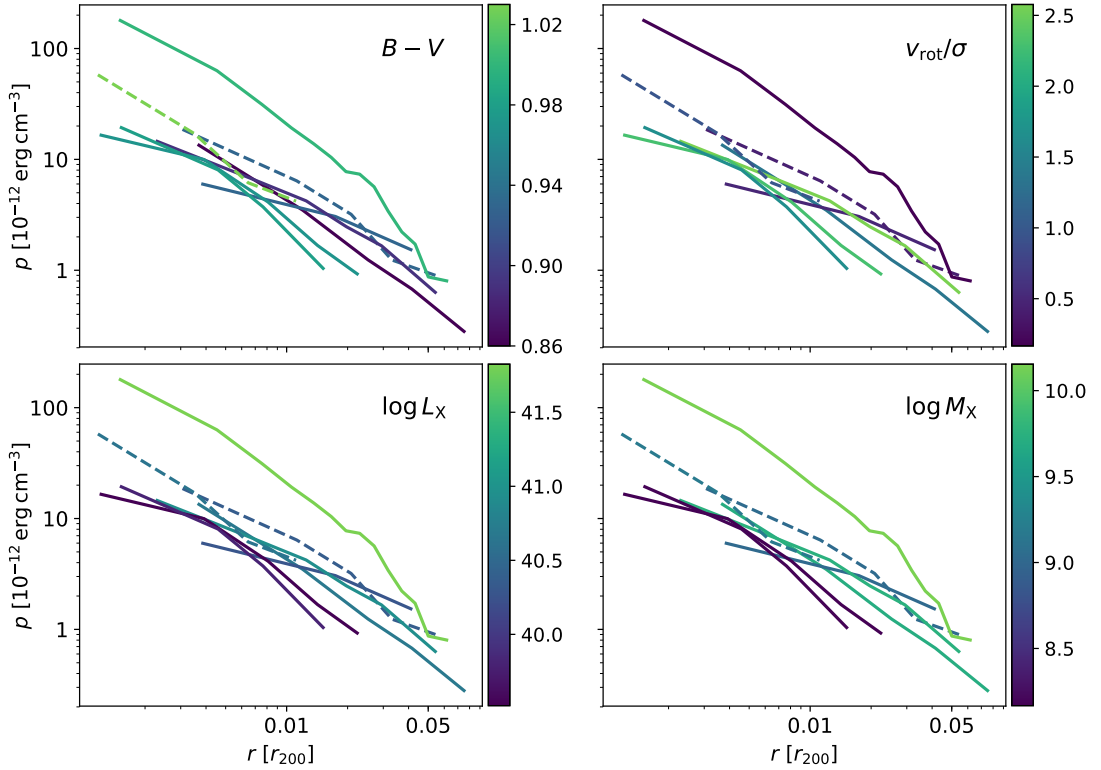


Figure 5.2: Pressure profiles in scale radius. The line colour is given by $B - V$ colour index (upper left), the ratio of rotational velocity and velocity dispersion (upper right), hot gas X-ray luminosity (lower left) and its mass (lower right). The scaled profiles with $r_{200,X}$, determined from X-ray observations, are shown as dashed lines, while those with known $r_{200,GC}$ are drawn with solid lines. The error bars are omitted for clarity.

5.2.3 Entropy

Central entropy in most of the studied S0 galaxies lies above that of elliptical galaxies, indicating that a centrally positioned heating mechanism should be present in these objects. Low star formation rate suggests that energy injection via winds of young stars and core-collapse supernovae is most likely incapable of providing sufficient heating. A plausible source of energy input would be connected to central AGN or type Ia SNe, presumably with an exception of NGC 4382, where the heating should have origin in processes excluding the central AGN, as discussed above. However, the hot atmosphere of this galaxy has a remarkably flat entropy profile which suggests that the halo is centrally overheated and convectively unstable in general.

The combined entropy profiles of rotating galaxies in our sample and three other objects with rotating discs of cold gas has been found to be flatter than what has been observed in cores of galaxy clusters and other elliptical galaxies. The power-law index measured here, $\Gamma = 0.46 \pm 0.05$, differs from the result of Babyk et al. (2018b) published for a sample of 6 galaxies consisting of spirals and lenticulars, $\Gamma = 0.74 \pm 0.06$. Their sample overlaps with our in two objects, namely NGC 4382 and NGC 5353, finding quantitatively similar profiles for the two. Their findings are based on data obtained by *Chandra*, performing a slightly different analysis using models provided within XSPEC spectral fitting package, but employing DSDEPROJ method for deprojection as well. Overall, the flattening in entropy profiles suggests relatively stronger heating in the rotationally supported atmospheres, possibly reflected in our findings concerning the systemically lower pressure in these systems.

5.3 Thermal stability

Central cooling times do not exceed ~ 0.5 Gyr and remain as low as ~ 1 Gyr out to 10 kpc, confirming that feedback is necessary to retain these hot atmospheres. The value of cooling time at 10 kpc for objects with observed cold gas phases is consistent with findings of Babyk et al. (2018c). This result, along with direct traces of AGN activity in several objects in our sample, raises the question of thermal stability of the gas.

The ratio of cooling time to free-fall time does not fall below ten at any radius, similarly to isolated ellipticals or brightest cluster galaxies (see e.g. Voit et al., 2018). In addition to the recent findings suggesting that the $t_{\text{cool}}/t_{\text{ff}} \approx 10$ represents rather a limit than a threshold for cooling, there are other reasons for not ruling out the possibility that the hot gas undergoes cooling via thermal instabilities: The free-fall time has been calculated under the assumption of hydrostatic equilibrium and, more importantly, the rotationally supported cooling clumps of gas would not be subjected to a free fall in the radial direction, owing to angular momentum conservation.

The calculation of C -ratio shows that the turbulence should be capable of generating density fluctuations prone to cooling. This outcome, yet consistent with the observed warm and cold phase discs, is dependent on our assumption of present velocity dispersion as the t_{eddy} scales with $\sigma_{v,L}^{-1}$. The velocity dispersion constrained from resonant scattering and line broadening has been measured by Ogorzalek et al. (2017)

in several elliptical galaxies using spectra from *XMM-Newton* Reflection Grating Spectrometer. The best-fitting 3D σ_v obtained for their whole sample is approximately 190 km s^{-1} , but with a large spread around this value for individual objects including also dispersions consistent with the value used here. This has been constrained for spectral extraction region width of $\sim 5 \text{ kpc}$ centred at the galaxy core, which is comparable to our systems, but neither of those studied by Ogorzalek et al. is a fast rotator. Although these predictions for the development of condensation are not strictly confined to $t_{\text{cool}}/t_{\text{eddy}} = 1$, the similarity of these two time-scales is required in order to observe the cooling multiphase gas. The velocity dispersion used in our calculations could, in reality, be significantly larger, and so would be the C -ratio. To obtain the true value of this parameter, spectroscopic measurements of the cold discs of e.g. the $[\text{C II}]\lambda 157 \mu\text{m}$ line, are necessary.

The cold gas reservoir could in principle be replenished by stellar ejecta. According to e.g. Voit and Donahue (2011), the gas ejected from stars should heat up and mix with the hot phase in systems with as low central density and star formation rate as in S0 galaxies studied here. Contrarily, the presence of cold gas with PAH molecules suggests a non-negligible role of winds of asymptotic giant branch stars (AGB) in cold gas deposition. A plausible explanation combining the precipitation from hot atmospheres and AGB winds has been recently presented by Li et al. (2019). Based on 3D hydrodynamical simulations, they suggest that cooling from the hot phase could be induced in the mixing layer of the dusty stellar wind and the surrounding hot gas, leading to preservation of these fragile particles.

Summary and conclusions

In this thesis, we present a study of X-ray emitting gaseous haloes of six lenticular galaxies. The sample was selected based on the kinematic state of these objects in order to study hot atmospheres subjected to effects of significant angular momentum. In Chapter 1, we introduce hot atmospheres of galaxies, focusing on their connection to colder gas phases and expected effects connected to their rotation. In Chapter 2, the studied sample is presented, with a primary focus on properties related to hot atmospheres, such as evidence for a presence of the AGN feedback, cold gas deposits, or star formation. Two more objects are added, a fast-rotating spiral galaxy and an elliptical in which the rotational support is negligible, both having extended emission from the hot gas. Chapter 3 is dedicated to a description of the analysis of X-ray spectra obtained by *XMM-Newton* EPIC instruments. As the quality of data allowed us to investigate the hot gas properties in several radial bins in each galaxy, we perform a deprojection analysis of these spectra and present the derived radial profiles in Chapter 4.

We find an alignment between the hot gas and stellar ellipticities with the X-ray ellipticity generally lower than that of stars, in an excellent agreement with our assumption of rotational support in these hot atmospheres and theoretical predictions. The combined entropy profile of seven rotating galaxies and three galaxies with indications for rotating atmospheres has been found to be flatter than what is observed in non-rotating ellipticals, suggesting relatively stronger heating in the central regions of these systems. We find a systemically lower gas pressure for all rotating galaxies in our sample when compared to non-rotating ellipticals. Remarkably, this dichotomy remains pronounced after scaling by total galaxy mass. We emphasize that this feature is common to all studied objects, having different properties related to manifestations of AGN activity, star formation rate or interaction with the surrounding environment. This outcome can be interpreted as a manifestation of outflows present in these atmospheres, in agreement with theoretical predictions of Pellegrini (2012).

Investigating the relation between hot haloes and the observed cold gas phases, we present the derived dimensionless parameters broadly adopted as being related to the thermal stability of hot atmospheres. The obtained ratio of cooling time and free-fall time, $t_{\text{cool}}/t_{\text{ff}} \gtrsim 10$ in all objects, is consistent with observations of ellipticals and even galaxy clusters. We also estimate the ratio of the cooling and turbulent time-scales and conclude that from the available data we cannot rule out that the discs of cold gas present in these objects have condensed out from the hot haloes.

APPENDIX A

Supplementary material

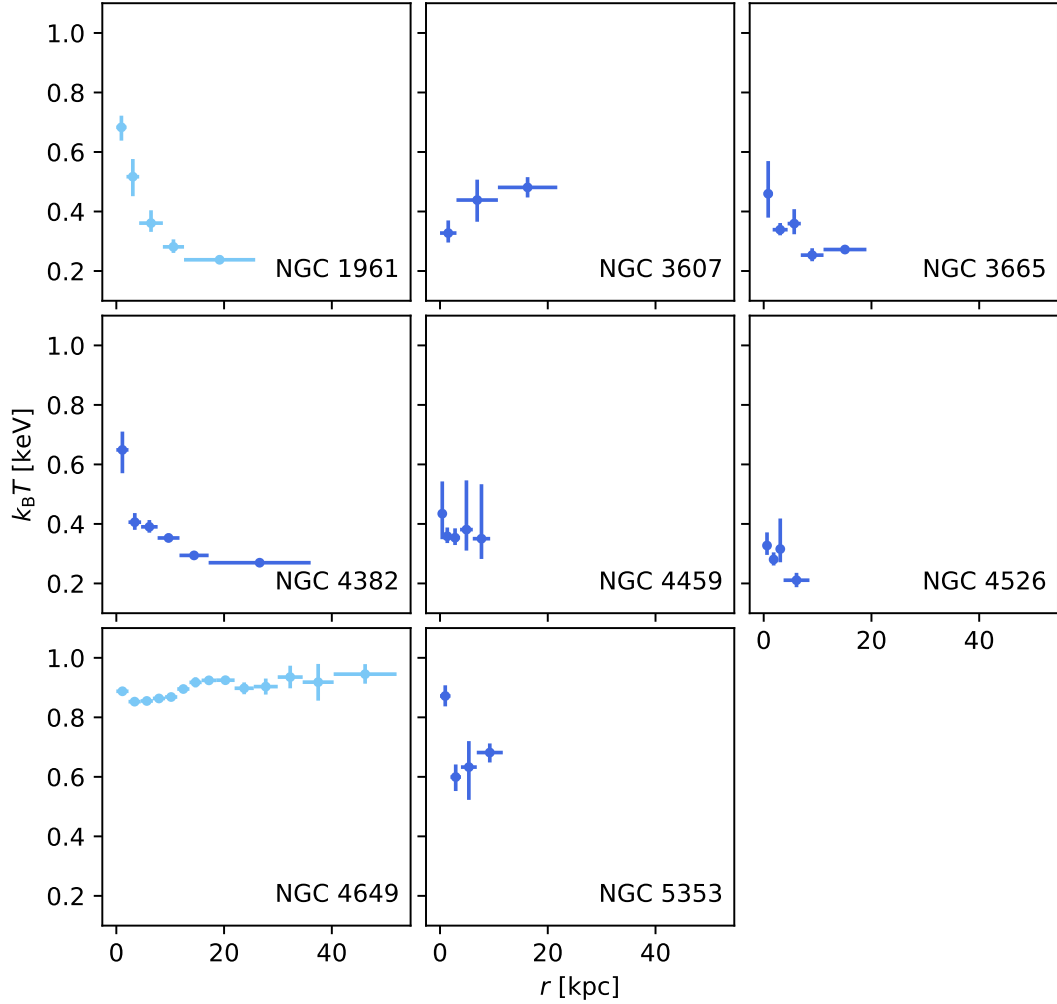


Figure A.1: Deprojected temperature profiles with metallicity fixed at $0.5 Z_{\odot}$ with the exception of NGC 4649 for which the metallicity is $0.7 Z_{\odot}$.

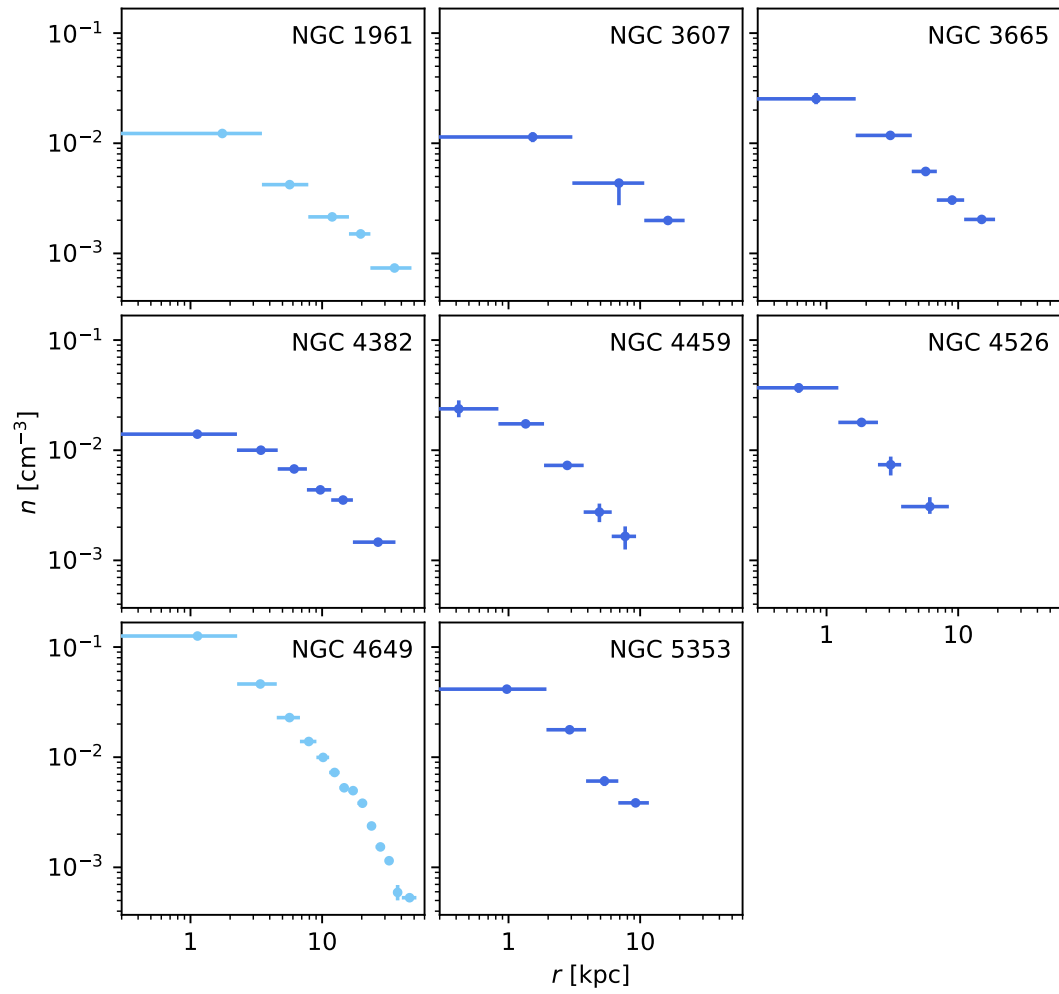


Figure A.2: Particle density profiles derived from deprojected spectra.

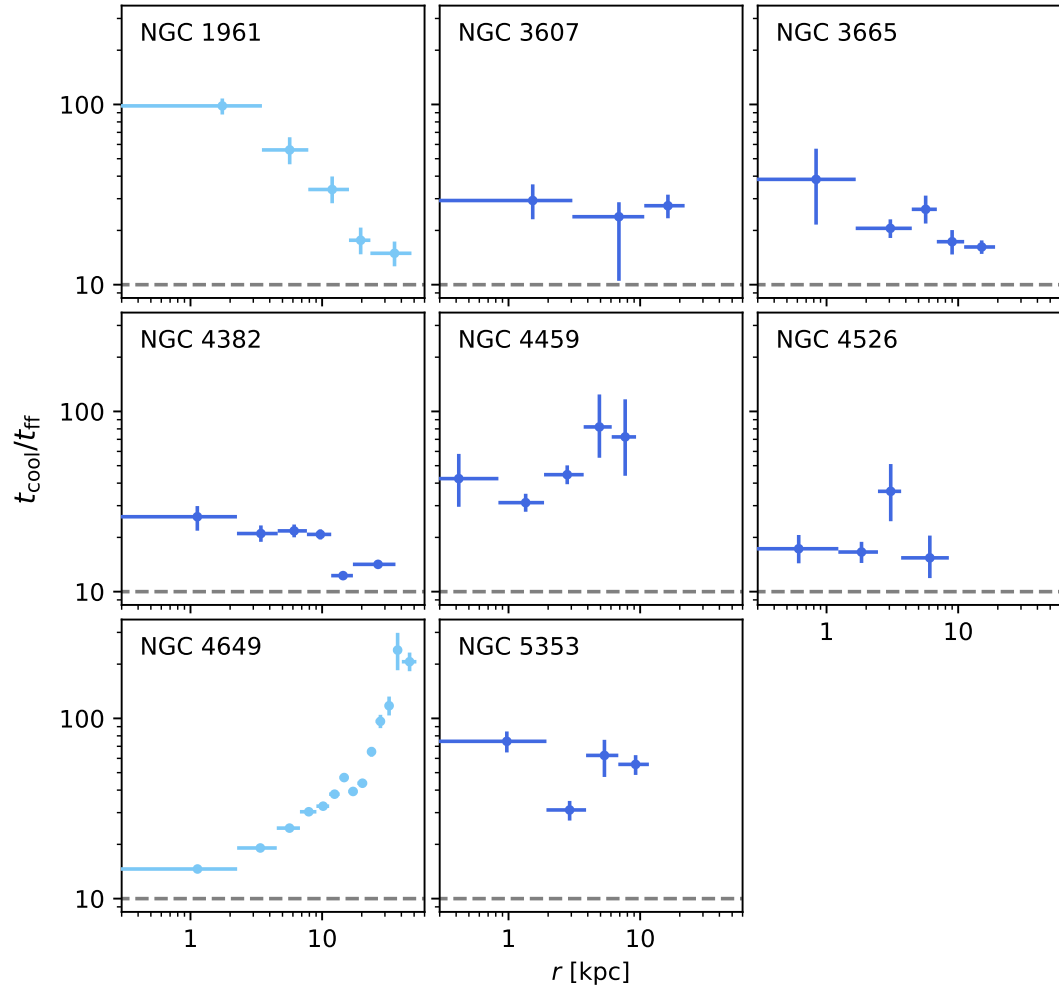


Figure A.3: Ratio of cooling time and free-fall time. The threshold of $t_{\text{cool}}/t_{\text{ff}} \approx 10$ is visualised as a dashed grey line.

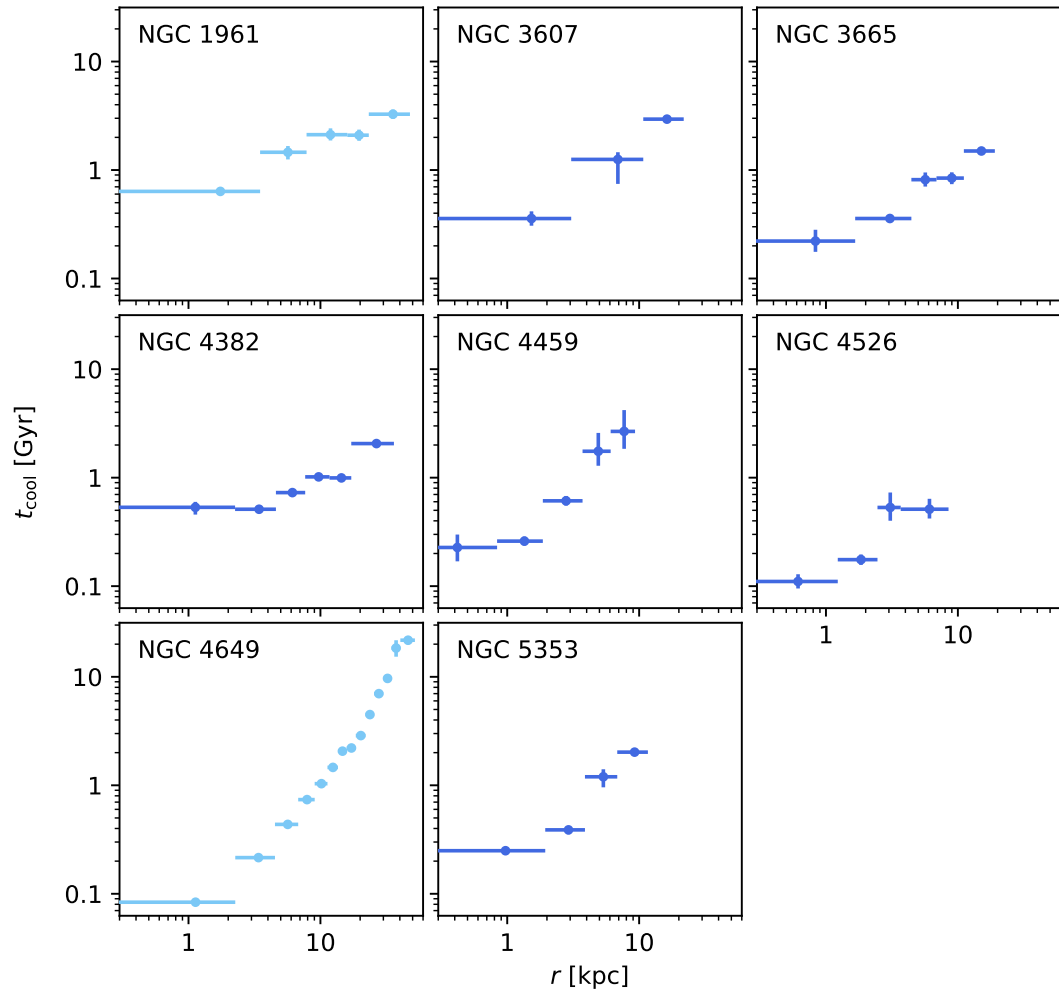


Figure A.4: Cooling time profiles derived from deprojected spectra.

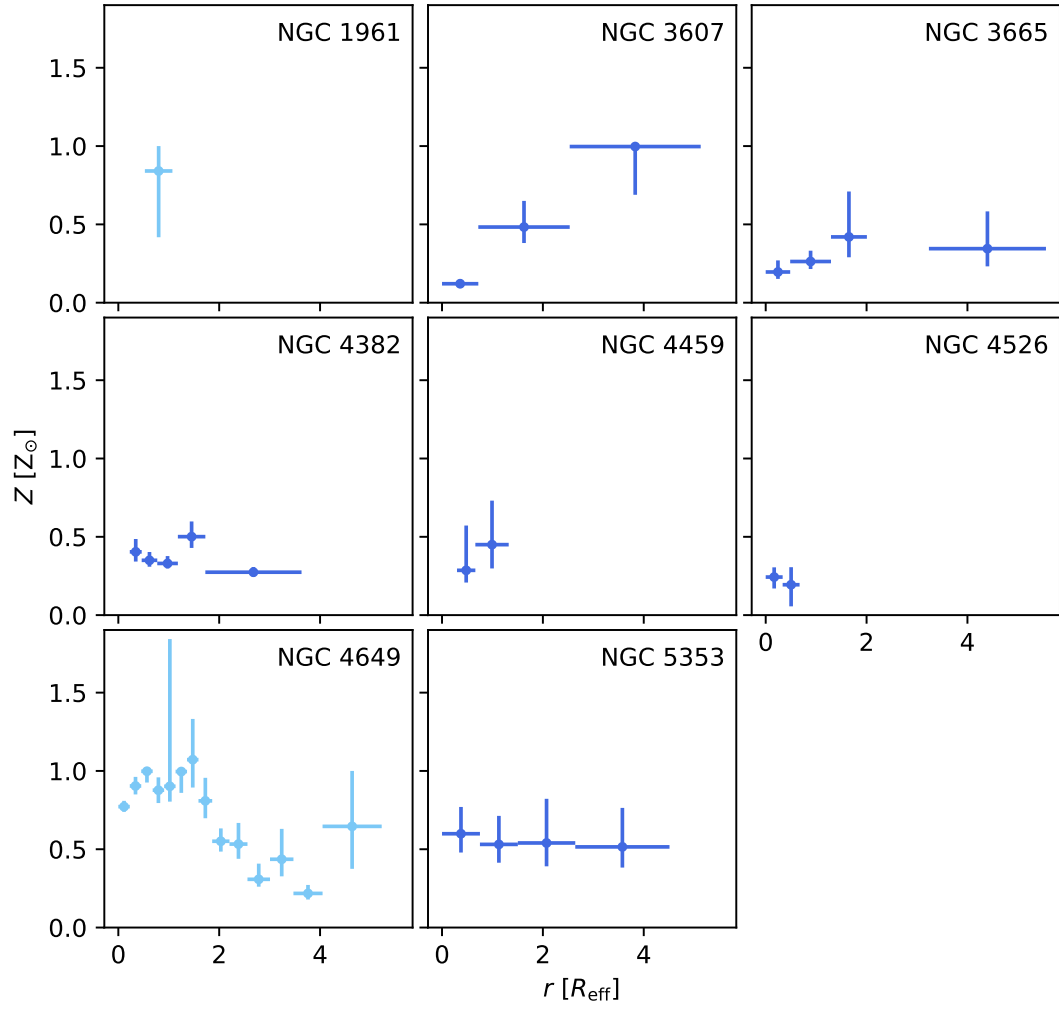


Figure A.5: Metallicity profiles derived from projected spectra.

Bibliography

- A. B. Alabi, D. A. Forbes, A. J. Romanowsky, J. P. Brodie, J. Strader, J. Janz, C. Usher, L. R. Spitler, S. Bellstedt, and A. Ferré-Mateu. The SLUGGS survey: dark matter fractions at large radii and assembly epochs of early-type galaxies from globular cluster kinematics. *MNRAS*, 468:3949–3964, Jul 2017.
- M. E. Anderson, E. Churazov, and J. N. Bregman. A deep XMM-Newton study of the hot gaseous halo around NGC 1961. *MNRAS*, 455(1):227–243, Jan 2016.
- Iu. V. Babyk, B. R. McNamara, P. E. J. Nulsen, M. T. Hogan, A. N. Vantyghem, H. R. Russell, F. A. Pulido, and A. C. Edge. X-Ray Scaling Relations of Early-type Galaxies. *ApJ*, 857(1):32, Apr 2018a.
- Iu. V. Babyk, B. R. McNamara, P. E. J. Nulsen, H. R. Russell, A. N. Vantyghem, M. T. Hogan, and F. A. Pulido. A Universal Entropy Profile for the Hot Atmospheres of Galaxies and Clusters within R_{2500} . *ApJ*, 862(1):39, Jul 2018b.
- Iu. V. Babyk, B. R. McNamara, P. D. Tamhane, P. E. J. Nulsen, H. R. Russell, and A. C. Edge. Origins of molecular clouds in early-type galaxies. *arXiv e-prints*, art. arXiv:1810.11465, Oct 2018c.
- D. J. Barnes, R. Kannan, M. Vogelsberger, and F. Marinacci. Radiative AGN feedback on a moving mesh: the impact of the galactic disc and dust physics on outflow properties. *arXiv e-prints*, art. arXiv:1812.01611, Dec 2018.
- H. Boehringer, W. Voges, A. C. Fabian, A. C. Edge, and D. M. Neumann. A ROSAT HRI study of the interaction of the X-ray emitting gas and radio lobes of NGC 1275. *MNRAS*, 264:L25–L28, Oct 1993.
- Á. Bogdán, W. R. Forman, M. Vogelsberger, H. Bourdin, D. Sijacki, P. Mazzotta, R. P. Kraft, C. Jones, M. Gilfanov, E. Churazov, and L. P. David. Hot X-Ray Coronae around Massive Spiral Galaxies: A Unique Probe of Structure Formation Models. *ApJ*, 772:97, Aug 2013.
- M. Brescia, S. Cavuoti, G. Longo, and V. De Stefano. A catalogue of photometric redshifts for the SDSS-DR9 galaxies. *A&A*, 568:A126, August 2014.
- T. J. Bridges and J. A. Irwin. Molecular gas in the Perseus cooling flow galaxy, NGC 1275. *MNRAS*, 300(4):967–976, Nov 1998.

- M. J. I. Brown, B. T. Jannuzi, D. J. E. Floyd, and J. R. Mould. The Ubiquitous Radio Continuum Emission from the Most Massive Early-type Galaxies. *ApJ*, 731(2):L41, Apr 2011.
- D. A. Buote. X-ray evidence for multiphase hot gas with nearly solar Fe abundances in the brightest groups of galaxies. *MNRAS*, 311(1):176–200, Jan 2000.
- A. Capetti, P. Kharb, D. J. Axon, D. Merritt, and R. D. Baldi. A Very Large Array Radio Survey of Early-Type Galaxies in the Virgo Cluster. *AJ*, 138:1990–1997, December 2009.
- M. Cappellari, E. Emsellem, D. Krajnović, R. M. McDermid, N. Scott, G. A. Verdoes Kleijn, L. M. Young, K. Alatalo, R. Bacon, L. Blitz, M. Bois, F. Bournaud, M. Bureau, R. L. Davies, T. A. Davis, P. T. de Zeeuw, P.-A. Duc, S. Khochfar, H. Kuntschner, P.-Y. Lablanche, R. Morganti, T. Naab, T. Oosterloo, M. Sarzi, P. Serra, and A.-M. Weijmans. The ATLAS^{3D} project - I. A volume-limited sample of 260 nearby early-type galaxies: science goals and selection criteria. *MNRAS*, 413:813–836, May 2011.
- R. Carrillo, J. Masegosa, D. Dultzin-Hacyan, and R. Ordoñez. A Multifrequency Catalog of LINERs. *Rev. Mexicana Astron. Astrofis.*, 35:187, Oct 1999.
- J. A. Carter and A. M. Read. The XMM-Newton EPIC background and the production of background blank sky event files. *A&A*, 464:1155–1166, March 2007.
- W. Cash. Parameter estimation in astronomy through application of the likelihood ratio. *ApJ*, 228:939–947, March 1979.
- A. Cavaliere and R. Fusco-Femiano. X-rays from hot plasma in clusters of galaxies. *A&A*, 49:137–144, May 1976.
- A. Cavaliere and R. Fusco-Femiano. The Distribution of Hot Gas in Clusters of Galaxies. *A&A*, 70:677, November 1978.
- E. Churazov, M. Brüggen, C. R. Kaiser, H. Böhringer, and W. Forman. Evolution of Buoyant Bubbles in M87. *ApJ*, 554(1):261–273, Jun 2001.
- E. Churazov, S. Sazonov, R. Sunyaev, W. Forman, C. Jones, and H. Böhringer. Supermassive black holes in elliptical galaxies: switching from very bright to very dim. *MNRAS*, 363(1):L91–L95, Oct 2005.
- S. Cielo, R. Bieri, M. Volonteri, A. Y. Wagner, and Y. Dubois. AGN feedback compared: jets versus radiation. *MNRAS*, 477(1):1336–1355, Jun 2018.
- F. Combes, L. M. Young, and M. Bureau. Molecular gas and star formation in the SAURON early-type galaxies. *MNRAS*, 377(4):1795–1807, Jun 2007.
- F. Combes, A. J. Baker, E. Schinnerer, S. García-Burillo, L. K. Hunt, F. Boone, A. Eckart, R. Neri, and L. J. Tacconi. Molecular gas in NUClei of GALaxies (NUGA). XII. The head-on collision in NGC 1961. *A&A*, 503:73–86, August 2009.

- J. J. Condon, W. D. Cotton, and J. J. Broderick. Radio Sources and Star Formation in the Local Universe. *AJ*, 124(2):675–689, Aug 2002.
- C. J. Conselice, III Gallagher, J. S., and R. F. G. Wyse. On the Nature of the NGC 1275 System. *AJ*, 122(5), Nov 2001.
- T. A. Davis, M. Bureau, M. Cappellari, M. Sarzi, and L. Blitz. A black-hole mass measurement from molecular gas kinematics in NGC4526. *Nature*, 494:328–330, Feb 2013.
- T. A. Davis, J. E. Greene, C.-P. Ma, J. P. Blakeslee, J. M. Dawson, V. Pandya, M. Veale, and N. Zabel. The MASSIVE survey - XI. What drives the molecular gas properties of early-type galaxies. *MNRAS*, page 847, Mar 2019.
- R. L. Dickman, Ronald L. Snell, and F. Peter Schloerb. Carbon Monoxide as an Extragalactic Mass Tracer. *ApJ*, 309:326, Oct 1986.
- M. Donahue, G. E. de Messières, R. W. O’Connell, G. M. Voit, A. Hoffer, B. R. McNamara, and P. E. J. Nulsen. Polycyclic Aromatic Hydrocarbons, Ionized Gas, and Molecular Hydrogen in Brightest Cluster Galaxies of Cool-core Clusters of Galaxies. *ApJ*, 732(1):40, May 2011.
- B. T. Draine. *Physics of the Interstellar and Intergalactic Medium*. 2011.
- R. J. H. Dunn, S. W. Allen, G. B. Taylor, K. F. Shurkin, G. Gentile, A. C. Fabian, and C. S. Reynolds. The radio properties of a complete, X-ray selected sample of nearby, massive elliptical galaxies. *MNRAS*, 404:180–197, May 2010.
- E. Emsellem, M. Cappellari, D. Krajnović, K. Alatalo, L. Blitz, M. Bois, F. Bournaud, M. Bureau, R. L. Davies, T. A. Davis, P. T. de Zeeuw, S. Khochfar, H. Kuntschner, P.-Y. Lablanche, R. M. McDermid, R. Morganti, T. Naab, T. Oosterloo, M. Sarzi, N. Scott, P. Serra, G. van de Ven, A.-M. Weijmans, and L. M. Young. The ATLAS^{3D} project - III. A census of the stellar angular momentum within the effective radius of early-type galaxies: unveiling the distribution of fast and slow rotators. *MNRAS*, 414:888–912, June 2011.
- ESA: XMM-Newton SOC. XMM-Newton Users Handbook, 2018. URL https://xmm-tools.cosmos.esa.int/external/xmm_user_support/documentation/uhb/. [Online; accessed 2019-05-14].
- P. B. Eskridge, G. Fabbiano, and D.-W. Kim. A Multiparametric Analysis of the Einstein Sample of Early-Type Galaxies. I. Luminosity and ISM Parameters. *The Astrophysical Journal Supplement Series*, 97:141, Mar 1995.
- A. C. Fabian. Cooling Flows in Clusters of Galaxies. *Annual Review of Astronomy and Astrophysics*, 32:277–318, Jan 1994.
- A. C. Fabian and P. E. J. Nulsen. Subsonic accretion of cooling gas in clusters of galaxies. *MNRAS*, 180:479–484, Aug 1977.

- G. J. Ferland, A. C. Fabian, and R. M. Johnstone. The Physical Conditions Within Dense Cold Clouds in Cooling Flows. *MNRAS*, 266:399, January 1994.
- L. Ferrarese and D. Merritt. A Fundamental Relation between Supermassive Black Holes and Their Host Galaxies. *ApJ*, 539(1):L9–L12, Aug 2000.
- L. Ferrarese, P. Côté, A. Jordán, E. W. Peng, J. P. Blakeslee, S. Piatek, S. Mei, D. Merritt, M. Milosavljević, J. L. Tonry, and M. J. West. The ACS Virgo Cluster Survey. VI. Isophotal Analysis and the Structure of Early-Type Galaxies. *The Astrophysical Journal Supplement Series*, 164:334–434, Jun 2006.
- G. B. Field. Thermal Instability. *ApJ*, 142:531, August 1965.
- A. Finoguenov and C. Jones. Chandra Observation of M84, a Radio Lobe Elliptical Galaxy in the Virgo Cluster. *ApJ*, 547(2):L107–L110, Feb 2001.
- A. Finoguenov, T. J. Ponman, J. P. F. Osmond, and M. Zimer. XMM-Newton study of $0.012 < z < 0.024$ groups - I. Overview of the IGM thermodynamics. *MNRAS*, 374:737–760, Jan 2007.
- W. Forman, P. Nulsen, S. Heinz, F. Owen, J. Eilek, A. Vikhlinin, M. Markevitch, R. Kraft, E. Churazov, and C. Jones. Reflections of Active Galactic Nucleus Outbursts in the Gaseous Atmosphere of M87. *ApJ*, 635(2):894–906, Dec 2005.
- A. Fruscione, J. C. McDowell, G. E. Allen, N. S. Brickhouse, D. J. Burke, J. E. Davis, N. Durham, M. Elvis, E. C. Galle, D. E. Harris, D. P. Huenemoerder, J. C. Houck, B. Ishibashi, M. Karovska, F. Nicastro, M. S. Noble, M. A. Nowak, F. A. Primini, A. Siemiginowska, R. K. Smith, and M. Wise. CIAO: Chandra’s data analysis system. In *Society of Photo-Optical Instrumentation Engineers (SPIE) Conference Series*, volume 6270 of Proc. SPIE, page 62701V, June 2006.
- E. Gallo, T. Treu, P. J. Marshall, J.-H. Woo, C. Leipski, and R. Antonucci. AMUSE-Virgo. II. Down-sizing in Black Hole Accretion. *ApJ*, 714(1):25–36, May 2010.
- M. Gaspari and E. Churazov. Constraining turbulence and conduction in the hot ICM through density perturbations. *A&A*, 559:A78, Nov 2013.
- M. Gaspari, P. Temi, and F. Brighenti. Raining on black holes and massive galaxies: the top-down multiphase condensation model. *MNRAS*, 466(1):677–704, Apr 2017.
- M. Gaspari, M. McDonald, S. L. Hamer, F. Brighenti, P. Temi, M. Gendron-Marsolais, J. Hlavacek-Larrondo, A. C. Edge, N. Werner, P. Tozzi, M. Sun, J. M. Stone, G. R. Tremblay, M. T. Hogan, D. Eckert, S. Ettori, H. Yu, V. Biffi, and S. Planelles. Shaken Snow Globes: Kinematic Tracers of the Multiphase Condensation Cascade in Massive Galaxies, Groups, and Clusters. *ApJ*, 854:167, February 2018.
- G. Gavazzi, G. Consolandi, S. Pedraglio, M. Fossati, M. Fumagalli, and A. Boselli. $H\alpha$ imaging observations of early-type galaxies from the ATLAS^{3D} survey. *A&A*, 611:A28, Mar 2018.

- K. Gebhardt, R. Bender, G. Bower, A. Dressler, S. M. Faber, A. V. Filippenko, R. Green, C. Grillmair, L. C. Ho, J. Kormendy, T. R. Lauer, J. Magorrian, J. Pinkney, D. Richstone, and S. Tremaine. A Relationship between Nuclear Black Hole Mass and Galaxy Velocity Dispersion. *ApJ*, 539(1):L13–L16, Aug 2000.
- G. Giuricin, C. Marinoni, L. Ceriani, and A. Pisani. Nearby Optical Galaxies: Selection of the Sample and Identification of Groups. *ApJ*, 543(1):178–194, Nov 2000.
- C. F. Goullaoud, J. B. Jensen, J. P. Blakeslee, C.-P. Ma, J. E. Greene, and J. Thomas. The MASSIVE Survey. IX. Photometric Analysis of 35 High-mass Early-type Galaxies with HST WFC3/IR. *ApJ*, 856:11, Mar 2018.
- R. Grossova, N. Werner, K. Rajpurohit, F. Mernier, K. Lakhchaura, K. Gabanyi, R. E. A. Canning, P. Nulsen, F. Massaro, M. Sun, T. Connor, A. King, S. W. Allen, R. Lyn-Salmon Frisbie, M. Donahue, and A. C. Fabian. Powerful AGN jets and unbalanced cooling in the hot atmosphere of IC 4296. *arXiv e-prints*, art. arXiv:1903.03198, Mar 2019.
- K. Gültekin, D. O. Richstone, K. Gebhardt, S. M. Faber, T. R. Lauer, R. Bender, J. Kormendy, and J. Pinkney. Is There a Black Hole in NGC 4382? *ApJ*, 741:38, Nov 2011.
- S. Haan, E. Schinnerer, C. G. Mundell, S. García-Burillo, and F. Combes. Atomic Hydrogen Properties of Active Galactic Nuclei Host Galaxies: H I in 16 Nuclei of Galaxies (NUGA) Sources. *AJ*, 135(1):232–257, Jan 2008.
- A. I. Harris, A. J. Baker, S. G. Zonak, C. E. Sharon, R. Genzel, K. Rauch, G. Watts, and R. Creager. CO $J = 1-0$ Spectroscopy of Four Submillimeter Galaxies with the Zpectrometer on the Green Bank Telescope. *ApJ*, 723(2):1139–1149, Nov 2010.
- C. M. Harrison. Impact of supermassive black hole growth on star formation. *Nature Astronomy*, 1:0165, Jul 2017.
- P. Hickson. Systematic properties of compact groups of galaxies. *ApJ*, 255:382–391, Apr 1982.
- M. T. Hogan, B. R. McNamara, F. Pulido, P. E. J. Nulsen, H. R. Russell, A. N. Vantyghem, A. C. Edge, and R. A. Main. Mass Distribution in Galaxy Cluster Cores. *ApJ*, 837(1):51, Mar 2017.
- P. J. Humphrey, D. A. Buote, F. Brighenti, K. Gebhardt, and W. G. Mathews. Reconciling stellar dynamical and hydrostatic X-ray mass measurements of an elliptical galaxy with gas rotation, turbulence and magnetic fields. *MNRAS*, 430(3):1516–1528, Apr 2013.
- J. A. Irwin, A. E. Athey, and J. N. Bregman. X-Ray Spectral Properties of Low-Mass X-Ray Binaries in Nearby Galaxies. *ApJ*, 587:356–366, April 2003.

- N. James, D.-W. Kim, G. Fabbiano, D. Forbes, and A. Alabi. The Mass of the Globular Cluster Systems of Early Type Galaxies as Proxy for the Total Galaxy Mass. *arXiv e-prints*, art. arXiv:1810.09475, Oct 2018.
- F. Jansen, D. Lumb, B. Altieri, J. Clavel, M. Ehle, C. Erd, C. Gabriel, M. Guainazzi, P. Gondoin, R. Much, R. Munoz, M. Santos, N. Schartel, D. Texier, and G. Vacanti. XMM-Newton observatory. I. The spacecraft and operations. *A&A*, 365:L1–L6, January 2001.
- T. H. Jarrett, T. Chester, R. Cutri, S. E. Schneider, and J. P. Huchra. The 2MASS Large Galaxy Atlas. *AJ*, 125(2):525–554, Feb 2003.
- A. Juráňová, N. Werner, M. Gaspari, K. Lakhchaura, P. E. J. Nulsen, M. Sun, R. E. A. Canning, S. W. Allen, A. Simionescu, J. B. R. Oonk, T. Connor, and M. Donahue. Cooling in the X-ray halo of the rotating, massive early-type galaxy NGC 7049. *MNRAS*, 484(2):2886–2895, Apr 2019.
- J. S. Kaastra, R. Mewe, and H. Nieuwenhuijzen. SPEX: a new code for spectral analysis of X & UV spectra. In K. Yamashita and T. Watanabe, editors, *UV and X-ray Spectroscopy of Astrophysical and Laboratory Plasmas*, pages 411–414, 1996.
- P. M. W. Kalberla, W. B. Burton, D. Hartmann, E. M. Arnal, E. Bajaja, R. Morras, and W. G. L. Pöppel. The Leiden/Argentine/Bonn (LAB) Survey of Galactic HI. Final data release of the combined LDS and IAR surveys with improved stray-radiation corrections. *A&A*, 440:775–782, September 2005.
- T. Kokusho, H. Kaneda, M. Bureau, T. Suzuki, K. Murata, A. Kondo, and M. Yamagishi. A star formation study of the ATLAS^{3D} early-type galaxies with the AKARI all-sky survey. *A&A*, 605:A74, Sep 2017.
- J. Kormendy. A critical review of stellar-dynamical evidence for black holes in galaxy nuclei. In J. Beckman, L. Colina, and H. Netzer, editors, *The Nearest Active Galaxies*, pages 197–218, January 1993.
- D. Krajnović, E. Emsellem, M. Cappellari, K. Alatalo, L. Blitz, M. Bois, F. Bournaud, M. Bureau, R. L. Davies, T. A. Davis, P. T. de Zeeuw, S. Khochfar, H. Kuntschner, P.-Y. Lablanche, R. M. McDermid, R. Morganti, T. Naab, T. Oosterloo, M. Sarzi, N. Scott, P. Serra, A.-M. Weijmans, and L. M. Young. The ATLAS^{3D} project - II. Morphologies, kinematic features and alignment between photometric and kinematic axes of early-type galaxies. *MNRAS*, 414:2923–2949, July 2011.
- M. Krips, A. Eckart, T. P. Krichbaum, J. U. Pott, S. Leon, R. Neri, S. García-Burillo, F. Combes, F. Boone, A. J. Baker, L. J. Tacconi, E. Schinnerer, and L. K. Hunt. NUclei of GALaxies. V. Radio emission in 7 NUGA sources. *A&A*, 464:553–563, Mar 2007.
- C. del P. Lagos, T. A. Davis, C. G. Lacey, M. A. Zwaan, C. M. Baugh, V. Gonzalez-Perez, and N. D. Padilla. The origin of the atomic and molecular gas contents of

- early-type galaxies - I. A new test of galaxy formation physics. *MNRAS*, 443(2): 1002–1021, Sep 2014.
- K. Lakhchaura, N. Werner, M. Sun, R. E. A. Canning, M. Gaspari, S. W. Allen, T. Connor, M. Donahue, and C. Sarazin. Thermodynamic properties, multiphase gas, and AGN feedback in a large sample of giant ellipticals. *MNRAS*, 481(4): 4472–4504, Dec 2018.
- K. Lakhchaura, F. Mernier, and N. Werner. Possible depletion of metals into dust grains in the core of the Centaurus cluster of galaxies. *A&A*, 623:A17, Mar 2019.
- Y. Li, G. L. Bryan, M. Ruszkowski, G. M. Voit, B. W. O’Shea, and M. Donahue. Cooling, AGN Feedback, and Star Formation in Simulated Cool-core Galaxy Clusters. *ApJ*, 811(2):73, Oct 2015.
- Y. Li, Y. Su, and C. Jones. X-ray cavities in the hot corona of the lenticular galaxy NGC 4477. *MNRAS*, 480(4):4279–4286, Nov 2018.
- Y. Li, G. L. Bryan, and E. Quataert. The Fate of AGB Wind in Massive Galaxies and the ICM. *arXiv e-prints*, art. arXiv:1901.10481, Jan 2019.
- E. Liuzzo, G. Giovannini, M. Giroletti, and G. B. Taylor. The Bologna complete sample of nearby radio sources. II. Phase referenced observations of faint nuclear sources. *A&A*, 505:509–520, Oct 2009.
- K. Lodders, H. Palme, and H.-P. Gail. Abundances of the Elements in the Solar System. *Landolt Börnstein*, 2009.
- D. M. Lucero and L. M. Young. A High-resolution Study of the Atomic Hydrogen in CO-rich Early-type Galaxies. *AJ*, 145:56, Mar 2013.
- D. Makarov and I. Karachentsev. Galaxy groups and clouds in the local ($z \sim 0.01$) Universe. *MNRAS*, 412(4):2498–2520, Apr 2011.
- D. Makarov, P. Prugniel, N. Terekhova, H. Courtois, and I. Vauglin. HyperLEDA. III. The catalogue of extragalactic distances. *A&A*, 570:A13, October 2014.
- G. A. Mamon. The nature of the nearest compact group of galaxies from precise distance measurements. *A&A*, 486(1):113–117, Jul 2008.
- M. McCourt, I. J. Parrish, P. Sharma, and E. Quataert. Can conduction induce convection? On the non-linear saturation of buoyancy instabilities in dilute plasmas. *MNRAS*, 413(2):1295–1310, May 2011.
- M. McDonald, S. Veilleux, D. S. N. Rupke, and R. Mushotzky. On the Origin of the Extended H α Filaments in Cooling Flow Clusters. *ApJ*, 721(2):1262–1283, Oct 2010.
- M. McDonald, S. Veilleux, and R. Mushotzky. The Effect of Environment on the Formation of H α Filaments and Cool Cores in Galaxy Groups and Clusters. *ApJ*, 731(1):33, Apr 2011.

- B. R. McNamara, H. R. Russell, P. E. J. Nulsen, M. T. Hogan, A. C. Fabian, F. Pulido, and A. C. Edge. A Mechanism for Stimulating AGN Feedback by Lifting Gas in Massive Galaxies. *ApJ*, 830(2):79, Oct 2016.
- F. Mernier, J. de Plaa, J. S. Kaastra, Y. Y. Zhang, H. Akamatsu, L. Gu, P. Kosec, J. Mao, C. Pinto, T. H. Reiprich, J. S. Sanders, A. Simionescu, and N. Werner. Radial metal abundance profiles in the intra-cluster medium of cool-core galaxy clusters, groups, and ellipticals. *A&A*, 603:A80, Jul 2017.
- T. Monfredini, H. M. Quitián-Lara, F. Fantuzzi, W. Wolff, E. Mendoza, A. F. Lago, D. A. Sales, M. G. Pastoriza, and H. M. Boechat-Roberty. Destruction and multiple ionization of PAHs by X-rays in circumnuclear regions of AGNs. *arXiv e-prints*, art. arXiv:1808.07626, Aug 2018.
- R. Morganti. The many routes to AGN feedback. *Frontiers in Astronomy and Space Sciences*, 4:42, Nov 2017.
- J. S. Mulchaey, D. S. Davis, R. F. Mushotzky, and D. Burstein. An X-Ray Atlas of Groups of Galaxies. *The Astrophysical Journal Supplement Series*, 145(1):39–64, Mar 2003.
- A. Negri, S. Posacki, S. Pellegrini, and L. Ciotti. The effects of galaxy shape and rotation on the X-ray haloes of early-type galaxies - II. Numerical simulations. *MNRAS*, 445(2):1351–1369, Dec 2014.
- N. Neininger, M. Guélin, H. Ungerechts, R. Lucas, and R. Wielebinski. Carbon monoxide emission as a precise tracer of molecular gas in the Andromeda galaxy. *Nature*, 395:871–873, October 1998.
- C. P. O’Dea, S. A. Baum, G. Privon, J. Noel-Storr, A. C. Quillen, N. Zufelt, J. Park, A. Edge, H. Russell, A. C. Fabian, M. Donahue, C. L. Sarazin, B. McNamara, J. N. Bregman, and E. Egami. An Infrared Survey of Brightest Cluster Galaxies. II. Why are Some Brightest Cluster Galaxies Forming Stars? *ApJ*, 681(2):1035–1045, Jul 2008.
- A. Ogorzalek, I. Zhuravleva, S. W. Allen, C. Pinto, N. Werner, A. B. Mantz, R. E. A. Canning, A. C. Fabian, J. S. Kaastra, and J. de Plaa. Improved measurements of turbulence in the hot gaseous atmospheres of nearby giant elliptical galaxies. *MNRAS*, 472(2):1659–1676, Dec 2017.
- K. Onishi, S. Iguchi, T. A. Davis, M. Bureau, M. Cappellari, M. Sarzi, and L. Blitz. WISDOM project - I. Black hole mass measurement using molecular gas kinematics in NGC 3665. *MNRAS*, 468:4663–4674, Jul 2017.
- E. O’Sullivan, F. Combes, P. Salomé, L. P. David, A. Babul, J. M. Vrtilik, J. Lim, V. Olivares, S. Raychaudhury, and G. Schellenberger. Cold gas in a complete sample of group-dominant early-type galaxies. *A&A*, 618:A126, Oct 2018.

- E. K. Panagoulia, A. C. Fabian, and J. S. Sanders. A volume-limited sample of X-ray galaxy groups and clusters - I. Radial entropy and cooling time profiles. *MNRAS*, 438(3):2341–2354, Mar 2014.
- P. Parma, H. R. de Ruiter, C. Fanti, and R. Fanti. VLA observations of low luminosity radio galaxies. I. Sources with angular size smaller than two arcminutes. *Astronomy and Astrophysics Supplement Series*, 64:135–171, Apr 1986.
- S. Pellegrini. Hot Gas Flows on Global and Nuclear Galactic Scales. In Dong-Woo Kim and Silvia Pellegrini, editors, *Astrophysics and Space Science Library*, volume 378 of *Astrophysics and Space Science Library*, page 21, Jan 2012.
- J. R. Peterson and A. C. Fabian. X-ray spectroscopy of cooling clusters. *Phys. Rep.*, 427:1–39, April 2006.
- J. R. Peterson, S. M. Kahn, F. B. S. Paerels, J. S. Kaastra, T. Tamura, J. A. M. Bleeker, C. Ferrigno, and J. G. Jernigan. High-Resolution X-Ray Spectroscopic Constraints on Cooling-Flow Models for Clusters of Galaxies. *ApJ*, 590(1):207–224, Jun 2003.
- F. Pizzolato and N. Soker. On the Nature of Feedback Heating in Cooling Flow Clusters. *ApJ*, 632(2):821–830, Oct 2005.
- A.-R. Pop, A. Pillepich, N. C. Amorisco, and L. Hernquist. Formation and incidence of shell galaxies in the Illustris simulation. *MNRAS*, 480(2):1715–1739, Oct 2018.
- D. Prasad, P. Sharma, and A. Babul. Cool Core Cycles: Cold Gas and AGN Jet Feedback in Cluster Cores. *ApJ*, 811(2):108, Oct 2015.
- G. W. Pratt, J. H. Croston, M. Arnaud, and H. Böhringer. Galaxy cluster X-ray luminosity scaling relations from a representative local sample (REXCESS). *A&A*, 498(2):361–378, May 2009.
- J. E. Pringle and A. King. *Astrophysical Flows*. 2007.
- F. A. Pulido, B. R. McNamara, A. C. Edge, M. T. Hogan, A. N. Vantyghem, H. R. Russell, P. E. J. Nulsen, I. Babyk, and P. Salomé. The Origin of Molecular Clouds in Central Galaxies. *ApJ*, 853(2):177, Feb 2018.
- M. J. Rees and J. P. Ostriker. Cooling, dynamics and fragmentation of massive gas clouds: clues to the masses and radii of galaxies and clusters. *MNRAS*, 179:541–559, Jun 1977.
- B. L. Refsdal, S. M. Doe, D. T. Nguyen, A. L. Siemiginowska, N. R. Bonaventura, D. Burke, I. N. Evans, J. D. Evans, A. Fruscione, E. C. Galle, J. C. Houck, M. Karovska, N. P. Lee, and M. A. Nowak. Sherpa: 1d/2d modeling and fitting in python. In Gaël Varoquaux, Stéfan van der Walt, and Jarrod Millman, editors, *Proceedings of the 8th Python in Science Conference*, pages 51 – 57, Pasadena, CA USA, 2009.

- J. Ridl, N. Clerc, T. Sadibekova, L. Faccioli, F. Pacaud, J. Greiner, T. Krühler, A. Rau, M. Salvato, M. L. Menzel, H. Steinle, P. Wiseman, K. Nandra, and J. Sanders. Cosmology with XMM galaxy clusters: the X-CLASS/GROND catalogue and photometric redshifts. *MNRAS*, 468(1):662–684, Jun 2017.
- S. Rosswog and M. Brüggen. *Introduction to High-Energy Astrophysics*. Cambridge University Press, 2007. ISBN 978-0-521-85769-7.
- V. C. Rubin, W. K. Jr. Ford, and M. S. Roberts. Extended rotation curves of high-luminosity spiral galaxies. V. NGC 1961, the most massive spiral known. *ApJ*, 230: 35–39, May 1979.
- H. R. Russell, J. S. Sanders, and A. C. Fabian. Direct X-ray spectral deprojection of galaxy clusters. *MNRAS*, 390:1207–1216, Nov 2008.
- P. Saikia, E. Körding, D. L. Coppejans, H. Falcke, D. Williams, R. D. Baldi, I. Mchardy, and R. Beswick. 15-GHz radio emission from nearby low-luminosity active galactic nuclei. *A&A*, 616:A152, Sep 2018.
- J. R. Sánchez-Sutil, A. J. Muñoz-Arjonilla, J. Martí, J. L. Garrido, D. Pérez-Ramírez, and P. Luque-Escamilla. A catalogue of ultra-luminous X-ray source coincidences with FIRST radio sources. *A&A*, 452:739–742, Jun 2006.
- E. Scannapieco and M. Brüggen. Subgrid Modeling of AGN-driven Turbulence in Galaxy Clusters. *ApJ*, 686(2):927–947, Oct 2008.
- P. Sharma, M. McCourt, E. Quataert, and I. J. Parrish. Thermal instability and the feedback regulation of hot haloes in clusters, groups and galaxies. *MNRAS*, 420: 3174–3194, March 2012.
- G. S. Shostak, E. Hummel, P. A. Shaver, J. M. van der Hulst, and P. C. van der Kruit. NGC 1961: Stripping of a supermassive spiral galaxy. *A&A*, 115:293–307, Nov 1982.
- K. Shurkin, R. J. H. Dunn, G. Gentile, G. B. Taylor, and S. W. Allen. Active galactic nuclei-induced cavities in NGC 1399 and NGC 4649. *MNRAS*, 383:923–930, Jan 2008.
- A. Simionescu, N. Werner, A. Finoguenov, H. Böhringer, and M. Brüggen. Metal-rich multi-phase gas in M 87. AGN-driven metal transport, magnetic-field supported multi-temperature gas, and constraints on non-thermal emission observed with XMM-Newton. *A&A*, 482(1):97–112, Apr 2008.
- S. L. Snowden and K. D. Kuntz. Analysis of XMM-Newton Data from Extended Sources and the Diffuse X-ray Background. In *American Astronomical Society Meeting Abstracts #217*, volume 43 of *Bulletin of the American Astronomical Society*, page 344.17, January 2011.

- S. Stierwalt, L. Armus, V. Charmandaris, T. Diaz-Santos, J. Marshall, A. S. Evans, S. Haan, J. Howell, K. Iwasawa, D. C. Kim, E. J. Murphy, J. A. Rich, H. W. W. Spoon, H. Inami, A. O. Petric, and V. U. Mid-infrared Properties of Luminous Infrared Galaxies. II. Probing the Dust and Gas Physics of the GOALS Sample. *ApJ*, 790(2):124, Aug 2014.
- L. Strüder, U. Briel, K. Dennerl, R. Hartmann, E. Kendziorra, N. Meidinger, E. Pfeffermann, C. Reppin, B. Aschenbach, W. Bornemann, H. Bräuninger, W. Burkert, M. Elender, M. Freyberg, F. Haberl, G. Hartner, F. Heuschmann, H. Hippmann, E. Kastelic, S. Kemmer, G. Kettenring, W. Kink, N. Krause, S. Müller, A. Oppitz, W. Pietsch, M. Popp, P. Predehl, A. Read, K. H. Stephan, D. Stötter, J. Trümper, P. Holl, J. Kemmer, H. Soltau, R. Stötter, U. Weber, U. Weichert, C. von Zanthier, D. Carathanassis, G. Lutz, R. H. Richter, P. Solc, H. Böttcher, M. Kuster, R. Staubert, A. Abbey, A. Holland, M. Turner, M. Balasini, G. F. Bignami, N. La Palombara, G. Villa, W. Buttler, F. Gianini, R. Lainé, D. Lumb, and P. Dhez. The European Photon Imaging Camera on XMM-Newton: The pn-CCD camera. *Astrophys. J.*, 365:L18–L26, January 2001.
- M. Sullivan, D. Le Borgne, C. J. Pritchett, A. Hodsman, J. D. Neill, D. A. Howell, R. G. Carlberg, P. Astier, E. Aubourg, D. Balam, S. Basa, A. Conley, S. Fabbro, D. Fouchez, J. Guy, I. Hook, R. Pain, N. Palanque-Delabrouille, K. Perrett, N. Regnault, J. Rich, R. Taillet, S. Baumont, J. Bronder, R. S. Ellis, M. Filiol, V. Lusser, S. Perlmutter, P. Riposte, and C. Tao. Rates and Properties of Type Ia Supernovae as a Function of Mass and Star Formation in Their Host Galaxies. *ApJ*, 648(2):868–883, Sep 2006.
- M. Sun. Hot gas in galaxy groups: recent observations. *New Journal of Physics*, 14(4):045004, Apr 2012.
- P. Temi, W. G. Mathews, F. Brighenti, and J. D. Bregman. Dust in Hot Gas: Far-Infrared Emission from Three Local Elliptical Galaxies. *ApJ*, 585:L121–L124, Mar 2003.
- E. Tempel, R. Kipper, A. Tamm, M. Gramann, M. Einasto, T. Sepp, and T. Tuvikene. Friends-of-friends galaxy group finder with membership refinement. Application to the local Universe. *A&A*, 588:A14, Apr 2016.
- R. C. Thomson. Shell formation in elliptical galaxies. *MNRAS*, 253:256, Nov 1991.
- G. R. Tremblay, F. Combes, J. B. R. Oonk, H. R. Russell, M. A. McDonald, M. Gaspari, B. Husemann, P. E. J. Nulsen, B. R. McNamara, S. L. Hamer, C. P. O’Dea, S. A. Baum, T. A. Davis, M. Donahue, G. M. Voit, A. C. Edge, E. L. Blanton, M. N. Bremer, E. Bulbul, T. E. Clarke, L. P. David, L. O. V. Edwards, D. Eggerman, A. C. Fabian, W. Forman, C. Jones, N. Kerman, R. P. Kraft, Y. Li, M. Powell, S. W. Randall, P. Salomé, A. Simionescu, Y. Su, M. Sun, C. M. Urry, A. N. Vantyghem, B. J. Wilkes, and J. A. ZuHone. A Galaxy-scale Fountain of Cold Molecular Gas Pumped by a Black Hole. *ApJ*, 865(1):13, Sep 2018.

- R. B. Tully and N. Trentham. Midlife Crises in Dwarf Galaxies in the NGC 5353/4 Group. *AJ*, 135(4):1488–1504, Apr 2008.
- M. J. L. Turner, A. Abbey, M. Arnaud, M. Balasini, M. Barbera, E. Belsole, P. J. Ben-
nie, J. P. Bernard, G. F. Bignami, M. Boer, U. Briel, I. Butler, C. Cara, C. Chabaud,
R. Cole, A. Collura, M. Conte, A. Cros, M. Denby, P. Dhez, G. Di Coco, J. Dowson,
P. Ferrando, S. Ghizzardi, F. Gianotti, C. V. Goodall, L. Gretton, R. G. Griffiths,
O. Hainaut, J. F. Hochedez, A. D. Holland, E. Jourdain, E. Kendziorra, A. Lagostina,
R. Laine, N. La Palombara, M. Lortholary, D. Lumb, P. Marty, S. Molendi, C. Pigot,
E. Poindron, K. A. Pounds, J. N. Reeves, C. Reppin, R. Rothenflug, P. Salvétat,
J. L. Sauvageot, D. Schmitt, S. Sembay, A. D. T. Short, J. Spragg, J. Stephen,
L. Strüder, A. Tiengo, M. Trifoglio, J. Trümper, S. Vercellone, L. Vigroux, G. Villa,
M. J. Ward, S. Whitehead, and E. Zonca. The European Photon Imaging Camera
on XMM-Newton: The MOS cameras : The MOS cameras. *A&A*, 365:L27–L35,
January 2001.
- G. M. Voit and M. Donahue. The Fate of Stellar Mass Loss in Central Cluster Galaxies.
ApJ, 738:L24, September 2011.
- G. M. Voit and M. Donahue. Cooling Time, Freefall Time, and Precipitation in the
Cores of ACCEPT Galaxy Clusters. *ApJ*, 799:L1, January 2015.
- G. M. Voit, C. P. Ma, J. Greene, A. Goulding, V. Pandya, M. Donahue, and M. Sun.
A General Precipitation-limited L_X -T-R Relation among Early-type Galaxies. *ApJ*,
853(1):78, Jan 2018.
- N. Werner, S. W. Allen, and A. Simionescu. On the thermodynamic self-similarity of
the nearest, most relaxed, giant ellipticals. *MNRAS*, 425:2731–2740, October 2012.
- N. Werner, J. B. R. Oonk, R. E. A. Canning, S. W. Allen, A. Simionescu, J. Kos, R. J.
van Weeren, A. C. Edge, A. C. Fabian, A. von der Linden, P. E. J. Nulsen, C. S.
Reynolds, and M. Ruszkowski. The Nature of Filamentary Cold Gas in the Core of
the Virgo Cluster. *ApJ*, 767(2):153, Apr 2013.
- N. Werner, J. B. R. Oonk, M. Sun, P. E. J. Nulsen, S. W. Allen, R. E. A. Canning,
A. Simionescu, A. Hoffer, T. Connor, M. Donahue, A. C. Edge, A. C. Fabian, A. von
der Linden, C. S. Reynolds, and M. Ruszkowski. The origin of cold gas in giant
elliptical galaxies and its role in fuelling radio-mode AGN feedback. *MNRAS*, 439:
2291–2306, April 2014.
- R. A. Wood, C. Jones, M. E. Machacek, W. R. Forman, A. Bogdan, F. Andrade-Santos,
R. P. Kraft, A. Paggi, and E. Roediger. The Infall of the Virgo Elliptical Galaxy M60
toward M87 and the Gaseous Structures Produced by Kelvin-Helmholtz Instabilities.
ApJ, 847:79, Sep 2017.
- L. M. Young, G. J. Bendo, and D. M. Lucero. Mid- to Far-Infrared Emission and Star
Formation in Early-Type Galaxies. *AJ*, 137:3053–3070, Feb 2009.

-
- L. M. Young, M. Bureau, T. A. Davis, F. Combes, R. M. McDermid, K. Alatalo, L. Blitz, M. Bois, F. Bournaud, M. Cappellari, R. L. Davies, P. T. de Zeeuw, E. Emsellem, S. Khochfar, D. Krajnović, H. Kuntschner, P.-Y. Lablanche, R. Morganti, T. Naab, T. Oosterloo, M. Sarzi, N. Scott, P. Serra, and A.-M. Weijmans. The ATLAS^{3D} project - IV. The molecular gas content of early-type galaxies. *MNRAS*, 414(2): 940–967, Jun 2011.
- L. M. Young, N. Scott, P. Serra, K. Alatalo, E. Bayet, L. Blitz, M. Bois, F. Bournaud, M. Bureau, A. F. Crocker, M. Cappellari, R. L. Davies, T. A. Davis, P. T. de Zeeuw, P.-A. Duc, E. Emsellem, S. Khochfar, D. Krajnović, H. Kuntschner, R. M. McDermid, R. Morganti, T. Naab, T. Oosterloo, M. Sarzi, and A.-M. Weijmans. The ATLAS^{3D} project - XXVII. Cold gas and the colours and ages of early-type galaxies. *MNRAS*, 444(4):3408–3426, Nov 2014.
- M. S. Yun, N. A. Reddy, and J. J. Condon. Radio Properties of Infrared-selected Galaxies in the IRAS 2 Jy Sample. *ApJ*, 554:803–822, Jun 2001.
- I. Zhuravleva, E. Churazov, A. A. Schekochihin, S. W. Allen, P. Arévalo, A. C. Fabian, W. R. Forman, J. S. Sanders, A. Simionescu, R. Sunyaev, A. Vikhlinin, and N. Werner. Turbulent heating in galaxy clusters brightest in X-rays. *Nature*, 515 (7525):85–87, Nov 2014.